Helsinki University of Technology
Department of Electrical and Communications Engineering
Optoelectronics Laboratory
Espoo, Finland 2006

GROWTH AND PROPERTIES OF COMPOUND SEMICONDUCTORS ON GERMANIUM SUBSTRATE

Lauri Knuuttila

Dissertation for the degree of Doctor of Science in Technology to be presented with due permission of the Department of Electrical and Communications Engineering, for public examination and debate in Auditorium TU1 at Helsinki University of Technology (Espoo, Finland) on the 5th of May, 2006, at 12 o´clock noon.

Helsinki University of Technology
Department of Electrical and Communications Engineering
Optoelectronics Laboratory

Distribution:
Helsinki University of Technology
Department of Electrical and Communications Engineering
Optoelectronics Laboratory
P.O.Box 3500
FIN-02015 HUT
FINLAND
Tel: +358 9 4511
Fax: +358 9 451 3128

ISBN 951-22-8109-0 (printed version)
ISBN 951-22-8110-4 (electronic version)

Picaset Oy
Helsinki 2006

HELSINKI UNIVERSITY OF TECHNOLOGY P. O. BOX 1000, FI-02015 TKK http://www.tkk.fi	ABSTRACT OF DOCTORAL DISSERTATION

Author Lauri Knuuttila

Name of the dissertation

Growth and properties of compound semiconductors on germanium substrate

Date of manuscript January 23, 2006	Date of the dissertation May 5, 2006
Article dissertation (overview + original articles)	Number of pages 69 + 55

Department	Department of Electrical and Communications Engineering
Laboratory	Optoelectronics laboratory
Field of research	Nanotechnology
Opponent	Prof. Heli Jantunen
Supervisor	Prof. Harri Lipsanen

Abstract

The aim of this thesis is to investigate the growth and characterisation of compound semiconductors on germanium (Ge) substrates. Also properties of detector applications and novel Ga(In)NAs compounds are presented on Ge substrates. The epitaxial growth is performed using metalorganic vapour phase epitaxy (MOVPE) technique.

The nucleation of zinc blende lattice compound semiconductors on the surface of diamond lattice Ge are highly affected by different growth conditions such as temperature, growth rate and partial pressure of source materials. Thus, thorough characterisation of the fabricated structures and optimisation of the growth parameters are required. Three-dimensional island formation was observed for initial growth phases of GaAs and In(Ga)As on Ge. The properties of the self-assembled islands were investigated using atomic force microscopy (AFM). $In_{0.5}Ga_{0.5}As$ islands grown at low temperature of 550°C showed a high areal density of 3.5×10^{10} cm^{-2} and uniformity in size. For grown GaAs layers the high initial island density and uniformity enables homogeneous coalescence of the islands as the growth is continued and results in smooth two-dimensional GaAs surfaces already at small layer thicknesses.

The crystal and optical properties of GaAs and Ga(In)NAs layers were investigated using high resolution X-ray diffraction (HRXRD), synchrotron X-ray topography (SXT) and photoluminescence (PL). In SXT measurements a 650 nm thick GaAs layer grown on Ge showed very small dislocation density of $250-500\,cm^{-2}$. The value is better than was found by SXT for the vapour pressure controlled Czochralski (VCz) grown GaAs substrates. The growth of GaAs on misoriented Ge substrate results in a tilt angle between the lattice planes of the substrate and the layer. For these structures it was shown that a specific HRXRD setup, in which the diffraction plane is parallel with the step edges on the Ge surface, enables accurate measurements and analyses of the structures.

From a GaInNAs multi-quantum well structure on Ge photoluminescence at telecommunication wavelength of 1.55 µm was obtained. From the HRXRD and PL results a nitrogen incorporation of about 5 % was determined for the quantum wells. Also for a GaAs/Ge matrix detector structure a record low leakage current of 3×10^{-9} A/cm^2 was obtained at 77 K. From arsenic diffusion based matrix detector fabricated on Ge substrate an excellent resolution of 220 eV at 5.9 keV and 400 eV at 60 keV was measured.

Keywords

Ge substrate, GaAs, GaInNAs, InAs, quantum well, quantum dot, compound semiconductor

ISBN (printed) 951-22-8109-0

ISBN (pdf) 951-22-8110-4

Publisher Helsinki University of Technology, Optoelectronics Laboratory

The dissertation can be read at http://lib.tkk.fi/Diss/2006/isbn9512281104/

TEKNILLINEN KORKEAKOULU PL 1000, 02015 TKK http://www.tkk.fi	VÄITÖSKIRJAN TIIVISTELMÄ

Tekijä Lauri Knuuttila

Väitöskirjan nimi

Yhdistepuolijohteiden kasvu germaniumalustakiteelle ja rakenteiden karakterisointi

Käsikirjoituksen jättämispäivämäärä 23.1.2006	Väitöstilaisuuden ajankohta 5.5.2006
Yhdistelmäväitöskirja (yhteenveto + erillisartikkelit)	Sivumäärä 69 + 55

Osasto	Sähkö- ja tietoliikennetekniikan osasto
Laboratorio	Optoelektroniikka
Tutkimusala	Nanoteknologia
Vastaväittäjä	Prof. Heli Jantunen
Työn valvoja	Prof. Harri Lipsanen

Tiivistelmä

Työssä käsitellään yhdistepuolijohteiden kasvua germaniumalustakiteille sekä rakenteiden karakterisointia. Työssä esitetään myös tuloksia germaniumiin perustuvista röntgendetektoreista ja germaniumille valmistetuista tietoliikenneaallonpituuksilla emittoivista GaInNAs-rakenteista. Yhdistepuolijohteet valmistettiin metallo-orgaanisella kaasufaasiepitaksilaitteistolla (MOVPE).

Kasvuolosuhteet kuten lämpötila, kasvunopeus ja lähtöaineiden osapaineet kasvureaktorissa vaikuttavat merkittävästi sinkkivälkehilaisten yhdistepuolijohteiden nukleaatioon timanttihilaisen germaniumin pinnalla. Näiden useiden kasvuparametrien optimointi edellyttää yksityiskohtaista rakenteiden karakterisointia. GaAs- ja In(Ga)As-yhdisteiden kolmiulotteista saarekemuodostumista tutkittiin atomivoimamikroskoopilla. Matalassa 550°C:een kasvulämpötilassa valmistettujen kooltaan hyvin homogeenisten itseorganisoituneiden $In_{0.5}Ga_{0.5}As$-saarekkeiden tiheydeksi mitattiin 3.5×10^{10} cm^{-2}. Suuri saareketiheys ja homogeeninen koko mahdollistavat saarekkeiden yhdistymisen pienempinä kun kasvatusta edelleen jatketaan. Tämä nopeuttaa valmistettavan GaAs kerroksen kasvumoodin muuttumista kaksiulotteiseksi kasvuksi ja tasainen pinta muodostuu pienemmillä kerrospaksuuksilla.

Näytteiden kidelaatua ja optisia ominaisuuksia tutkittiin käyttämällä röntgendiffraktometriä, röntgentopografia- ja fotoluminesenssimittauksia. Röntgendiffraktiossa vaikeutena ovat Ge-alustakiteen ja epitaktisten kerrosten suhteessa toisiinsa kallistuneet hilatasot. Rakenteiden mittaamisen mahdollistaa erityinen mittausgeometria, jossa alustakiteen askelreunat yhtyvät diffraktiotasoon. Röntgentopografialla mitattiin germaniumille valmistetusta 650 nm:n paksuisesta GaAs-kerroksesta erittäin alhainen $250 - 500$ cm^{-2} dislokaatiotiheys.

Germaniumille valmistetusta GaInNAs-kvanttikaivokerrosrakenteesta mitattiin emissiota 1,55 µm aallonpituudella, joka on yleisesti käytössä tietoliikennekomponenteissa. Perinteisesti komponentit näin pitkille aallonpituuksille joudutaan valmistamaan InP:iin perustuvista yhdisteistä. Röntgendiffraktio- ja fotoluminesenssimittauksista GaInNAs-kvanttikaivojen typpipitoisuudeksi määritettiin 5 %. GaAs/Ge-matriisidetektorirakenteille mitattiin ennätyspieni vuotovirrantiheys 3×10^{-9} A/cm^2 77 K:n lämpötilassa ja arseenidiffuusiolla valmistetuista Ge-matriisidetektoreista mitattiin erinomainen 220 eV resoluutio 5,9 keV energialla ja 400 eV resoluutio 60 keV energialla.

Asiasanat

Ge alustakide, GaInNAs, InAs, kvanttikaivo, kvanttipiste, yhdistepuolijohde

ISBN (painettu) 951-22-8109-0

ISBN (pdf) 951-22-8110-4

Julkaisija Teknillinen korkeakoulu, Optoelektroniikan laboratorio

Luettavissa verkossa osoitteessa http://lib.tkk.fi/Diss/2006/isbn9512281104/

Preface

The work presented in this thesis has been carried out in Optoelectronics Laboratory of Helsinki University of Technology between 2000 and 2006. I want to express my gratitude to Professors Turkka Tuomi and Harri Lipsanen for an opportunity to work in the field of semicondutor epitaxy and for the support during the time. I am grateful to Docent Markku Sopanen and Dr. Juha Toivonen for introducing MOVPE technique to me and for providing the guidance especially in the beginning. M.Sc. Marco Mattila I would like to thank for setting up the new MOVPE laboratory with me in the Micronova building and also M.Sc. Outi Reentilä for the collaboration in the epitaxial growth of sometimes mysterious three-five nitrides.

I want to thank Prof. Patrick McNally from the Dublin City University, soon to be Dr. Juha Riikonen, M.Sc. Aapo Lankinen, M.Sc. Antti Säynätjoki and M.Sc. Pasi Kostamo for the cooperation in the various places and occasions. The Graduate school of electronics, telecommunications and automation is acknowledged for their financial support of this work.

I have enjoyed the company of many people working in the Optoelectronics Laboratory, thanks to you, especially the enthusiasm of Dr. Karri Varis provided many moments of true inspirations during the time. Thanks to friends outside the office and to Leo for taking care of outdoor activities and clearing the thoughts.

I want to express great gratitude to my parents for the constant support and encouragement. My two brothers I thank for showing great example how this is done. Finally, my greatest gratitude and love to Liisa for always believing in me and loving me back.

Espoo, March 2006 Lauri Knuuttila

Table of Contents

List of Publications

This thesis consists of an overview and of the following publications which are referred to in the text by their Roman numerals.

I L. Knuuttila, A. Lankinen, J. Likonen, H. Lipsanen, X. Lu, P. McNally, J. Riikonen, and T. Tuomi, *Low Temperature Growth GaAs on Ge*, Japanese Journal of Applied Physics **44**, 7777–7784 (2005).

II L. Knuuttila, K. Kainu, M. Sopanen, and H. Lipsanen, *In(Ga)As quantum dots on Ge substrate*, Journal of Materials Science: Materials in Electronics **14**, 349–352 (2003).

III L. Knuuttila, T. Korkala, M. Sopanen, and H. Lipsanen, *Self-assembled In(Ga)As islands on Ge*, Journal of Crystal Growth **272**, 221–226 (2004).

IV T. Tuomi, L. Knuuttila, J. Riikonen, P. McNally, W. Chen, J. Kanatharana, M. Neubert, and P. Rudolph, *Synchrotron X-ray topography of undoped VCz GaAs crystals*, Journal of Crystal Growth **237-239**, 350–355 (2002).

V A. Lankinen, L. Knuuttila, T. Tuomi, P. Kostamo, A. Säynätjoki, J. Riikonen, H. Lipsanen, P. McNally, H. Sipilä, S. Vaijärvi, and D. Lumb, *Synchrotron X-ray topography study of defects in epitaxial GaAs on high-quality Ge*, accepted for publication in Nuclear Instruments and Methods in Physics Research Section A, 4 pages.

VI J. Toivonen, T. Tuomi, J. Riikonen, L. Knuuttila, T. Hakkarainen, M. Sopanen, H. Lipsanen, P. McNally, W. Chen, and D. Lowney, *Misfit dislocations in GaAsN/GaAs interface*, Journal of Materials Science: Materials in Electronics **14**, 267–270 (2003).

VII L. Knuuttila, O. Reentilä, M. Mattila, and H. Lipsanen, *Comparison of Ge and GaAs Substrates for Metalorganic Vapor Phase Epitaxy of GaIn(N)As Quamtum Wells*, Japanese Journal of Applied Physics **44**, L1475–L1477 (2005).

VIII P. Kostamo, A. Säynätjoki, L. Knuuttila, H. Lipsanen, H. Andersson, K. Banzuzi, S. Nenonen, H. Sipilä, S. Vaijärvi, and D. Lumb, *Ge/GaAs heterostructure matrix detector*, accepted for publication in Nuclear Instruments and Methods in Physics Research Section A, 4 pages.

Author's contribution

The author has written the manuscripts for publications I, II, III, and VII, and he has contributed to the data analysis and manuscripts for publications IV, V, VI, and VIII. The author has designed sample structures, growth parameters and completed the growth for the samples in publications I, II, III, V, VII, and VIII where he has especially focused on the growth aspect of compound semiconductors on Ge substrates and on characterisation of these structures.

The author has performed the surface morphology studies for the publications I, II, and III, and he has done the optical measurements for the publications I, II, and VII. The X-ray diffraction studies for the publications I, II, and VII were performed by the author. The synchrotron X-ray topography studies for publication I, IV, and V were mainly carried out by the author and assisted by the co-authors of publications. For the publication VI the author participated in the fabrication of the samples and in the synchrotron X-ray topography studies.

1 Introduction

Semiconductors are practically found almost from every electrical device. The continuous research of novel material solutions and development of fabrication methods enables new and more advanced devices in our live frequently. Optical telecommunication technology and optical data storage is based on semiconductor lasers and light emitting devices (LEDs) are gradually substituting incandescent lamps in various applications. These advanced components require nearly perfectly controlled epitaxial growth of compound semiconductors. The ability to control the alloying of binary compounds and the possibility to fabricate coherently strained thin layers with sharp interfaces enables tailoring of the electronic band structure ($\sim$ i.e., "colour of light") of compound semiconductors. Semiconductors are also essential when receiving radiation, that is, in detecting instruments and in solar cells. Using compound semiconductors the performance of these devices can be further enhanced.

1.1 Germanium material

The element germanium was discovered by a German chemist C. Winkler in 1886. Prior to that in 1871 the existence of an element later know as germanium was predicted by D. Mendeleev. Germanium is a group four element along with carbon, silicon, tin and lead from which Ge and Si are widely used as semiconductors. Ge has a diamond lattice that is composed of two interpenetrating face centred cubic (FCC) lattices, one displaced 1/4 of a lattice constant in each direction from the other. Each site is tetrahedrally coordinated with four other sites in the other sublattice. Zinc blende lattice, e.g., GaAs is almost similar to the diamond structure but the two FCC sublattices are of different atoms. The main uses of Ge material are transistors, dopant material in optical fibres and substrates of epitaxial growth of III-V compounds. The very first transistor in 1947 was made of

Ge and Ge has superior transport properties compared to Si but lacks a high quality oxide for passivation [1]. Recently several studies have been published demonstrating high-k gate dielectric metal-oxide-semiconductor (MOS) transistors based on Ge [2–5].

1.2 Germanium heteroepitaxy

When considering epitaxial growth the two vital issues are the crystal structure and the lattice constant of the substrate material. The lattice constant of non-polar Ge is 5.6578 Å at room temperature having only a 0.07 % difference if compared to polar GaAs lattice constant of 5.6537 Å. Different lattice constants and photon energies of the most relevant materials are presented in Fig. 1.1. The suitable value of Ge lattice constant enables several semiconductor compounds to be grown on it without any significant strain field to be built up. Currently the most important application of germanium substrates are solar cells used in satellite's power supply. Also Hall sensors, detectors and light emitting diodes are manufactured on Ge and its lattice constant enables almost strain free growth of distributed AlAs/GaAs Bragg reflectors for vertical cavity structures. The initial growth of GaAs on Si is very analogous with polar-on-nonpolar growth cycle if compared to GaAs on Ge [6–11]. Unfortunately, the small lattice difference is not the case with GaAs-Si system. However, compositionally graded Si_xGe_{1-x} layers on Si substrates appear to be solution as a graded lattice constant interlayer that can eliminate the mismatch between several III-V/Si materials [12, 13]. Using this Si_xGe_{1-x} step grading so called virtual Ge substrates with dislocation densities of 1×10^6 cm^{-2} have been demonstrated [12, 14]. This also encourages further to study heteroepitaxy on Ge substrates.

For many applications it is possible to choose between the GaAs and Ge substrate. Compared to GaAs substrates Ge substrates are available in larger size up to 14" diameter wafers with very small dislocation density. For GaAs wafers corresponding values are 6" and lowest dislocation densities are around 1500 cm^{-2} (publication IV). Ge wafers are also available as very high purity with impurity concentration of about 10^{10} cm^{-3}. Ge has higher mechanical strength, thereby allowing thinner substrates that reduce cost and weight for instance in solar cell applications where large area is a necessity. The weight reduction is especially substantial for the space solar cells. Ge has higher thermal conductivity than GaAs providing better cooling for electronic components and cooling can be further enhanced using the thinner substrates. Also important viewpoint is that Ge

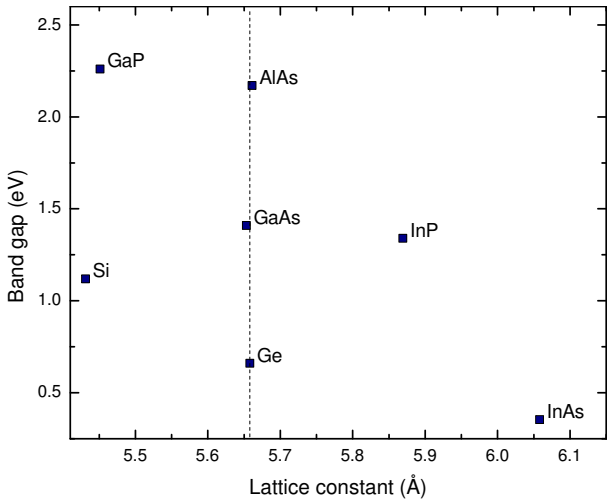

Figure 1.1. Band gaps and lattice constants of the most relevant semiconductor materials related to germanium.

is a non-toxic element whereas, e.g., with GaAs caution is necessary. The reason that GaAs is by far more popular as substrate material than Ge in most optoelectronic components is the ease of the homoepitaxy and the fact that there are two fundamental difficulties concerning polar on non-polar heteroepitaxy: i) interfacial diffusion during the high temperature growth, and ii) formation of antiphase domains (APD). The diffusion of Ga and As into the Ge substrate during the growth is known to create p- and n-type doping, respectively. Arsenic has larger diffusion coefficient than Ga and diffuses deeper into Ge possibly introducing a p-n junction into Ge [15, 16]. Also Ge diffuses into epitaxial GaAs creating impurities. The diffusion can be reduced using lower growth temperatures (publication I), higher growth rates [17], and suitable buffer layers [18]. The second difficulty, the APDs are domains of opposite orientation and are separated by an antiphase boundaries (APBs) consisting of As-As or Ga-Ga bonds. The APDs are formed by either i) incomplete prelayer coverage, where the growth starts from Ga or As atom at different surface areas on Ge or ii) by steps of odd height on Ge surface. The formation of APDs can be effectively hindered using misoriented Ge substrates. These issues are more precisely presented in chapter 3.3. The epitaxial growth on Ge substrates is mainly performed by metalorganic vapour phase epitaxy (MOVPE) and molecular beam epitaxy (MBE). Several studies concerning GaAs heteroepitaxy on Ge have been published using MOVPE [17, 19–29] or MBE [15, 30–38].

1.3 Structure of thesis

The aim of this overview is to present a summary of results gained in publications I-VIII, where the growth of GaAs based heterostructures on Ge substrates is described from the very first nucleation phases to the actual applications. The thesis mainly covers experimental viewpoint to the characterisation and growth by MOVPE of the presented heterostructures. The following chapter focuses on the background of MOVPE technique and considers more extensively surface kinetics limited growth regime, which plays a crucial part in most grown structures. The chapter also compares MBE and MOVPE techniques and briefly describes the MOVPE equipment used in this study. In the third chapter nucleation of different compound semiconductors on Ge surface is presented. In the same chapter for the GaAs material the phases of nucleation and initial growth conditions resulting into high quality epitaxial layers on Ge are summed up. Chapter 4 introduces high resolution X-ray diffraction method and its setup to characterise tilted structures on misoriented substrates. In the same chapter high resolution X-ray diffraction topography technique using synchrotron radiation is described and its application to the study of dislocations is presented. Also in this chapter optical characterisation using photoluminescence analyses is presented. In chapter 5 the most important applications fabricated on Ge substrates are introduced including a short review of solar cells and results from Ge matrix detectors as well properties of dilute nitride GaAsN layers and GaInNAs quantum well structures on Ge. Finally, the discussion is summarised in chapter 6

2 Metalorganic vapour phase epitaxy

Metalorganic vapour phase epitaxy is a non-equilibrium growth technique suitable for complex electronic structures. The technique was first development by Manasevit *et al.* at the end of the 1960's to grow single crystal GaAs films on insulator substrates [39]. Since that MOVPE has become the main fabrication technique over liquid phase epitaxy (LPE) and MBE for III-V semiconductors including gallium nitride materials.

In MOVPE technique the atom of interest is obtained by a chemical reaction from a metalorganic molecule. The metalorganic source materials have a high vapour pressure and can be transported into the growth reactor via high-purity carrier gas, usually hydrogen. The source materials, i.e., precursors decompose in the growth reactor just above and on a heated susceptor and the adatoms diffuse to the surface of the growth substrate and nucleate forming, e.g., a GaAs crystal.

The growth pressure range in MOVPE is usually from atmospheric pressure down to 10 hPa. Group III precursors in MOVPE technique are metalorganic compounds such as trimethylgallium (TMGa, i.e., $Ga(CH_3)_3$). For group V precursors both metalorganics such as tertiarybutylarsine (TBAs, i.e., $(CH_3)_3CAsH_2$) and hydrides such as AsH_3 can be used. The hydrides are more cost effective and especially favoured in industrial production. However, the metalorganic precursors are much safer and suitable for low temperature growth, as in this study, since their decomposition temperature is lower. In MOVPE technique it is essential that high purity metalorganic source materials, containing less than 1 ppm of individual impurities such as copper and iron, are available. From the carrier gas, which usually also acts as a growth ambient, impurities are removed very effectively using diffusion through a palladium foil (used for the growths in publications II, III, and VI), or using passive solutions based on organometallic polymers with

reactive functional groups (used for the growths in publications I, V, VII, and VIII). No difference in purity between these two purification methods was noticed.

2.1 Growth regimes

In MOVPE growth three different regimes are recognised, that depend mainly on the growth temperature: i) surface kinetics limited growth, ii) mass transport limited growth and iii) temperature limited growth. The separation between different regimes is not always well-defined and two growth regimes can occur partly simultaneously. Growth can be separated into thermodynamics, kinetics, hydrodynamics and mass transport processes. Fig. 2.1 shows the different simplified processes that occur during the growth in MOVPE. The thermodynamics determines the driving force for the growth and kinetics defines the rate of different processes. Hydrodynamics controls the flow of the source materials close to the substrate and mass transport describes the diffusion through the boundary layer, where the carrier gas flow velocity is decreased towards solid/vapour interface.

In the temperature limited growth regime, which occurs at high temperatures above $\sim 800^{\circ}$C, the deposition is mainly affected by the desorption of atoms from the growth surface. Also due to the high temperature an

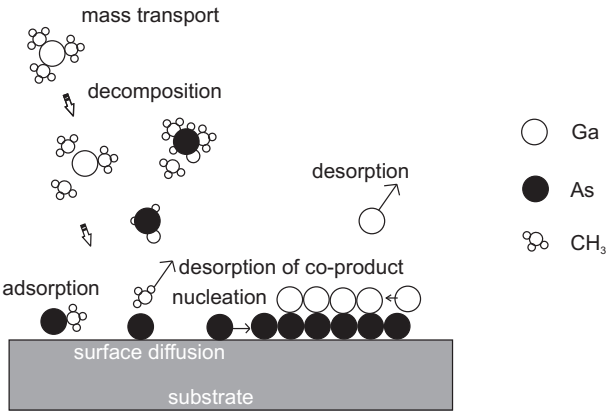

Figure 2.1. Fundamental processes occurring in the MOVPE growth.

increased number of prereactions is likely to happen. Usually the growth of gallium nitride based layers is performed at these elevated temperatures.

Mass transport limited growth is referred to as conventional growth regime and occurs roughly between $550 - 800°C$. There the input partial pressure, i.e., the flux of group III precursors defines the growth rate and composition of the forming epitaxial layer. The growth rate is roughly independent of temperature as the mass transport controls the diffusion across the boundary layer. The surface reactions of group III atoms are fast and the surface desorption is minimal. The group V atom incorporation is self-limiting and their input partial pressure is maintained higher than group III partial pressure. This indicates that the layer growth is typically insensitive to the input V/III ratio in the mass transport limited regime.

The challenging and interesting growth regime is the surface kinetics limited mode. The growth temperatures in this regime are lower than in the mass transport limited growth regime starting from about 600°C and reaching as low as 400°C. Difficulties are encountered as the precursors decompose incompletely, and co-products are not necessarily desorbed from the sample surface. For example, incomplete decomposition of TMGa induces reduced growth rate and compositional modifications in InGaAs epitaxial layers. As already mentioned above, TBAs decomposes more efficiently at lower temperatures than AsH_3 and also TEGa can be used instead of TMGa [40]. The group V atom incorporation is self-limiting but the input V/III molar flow ratio has only a narrow growth window. A thorough study about metalorganic source materials for vapour phase epitaxy is presented in a review article by A. Jones [41]. Most of the dilute nitride and quantum dot (QD) structures are grown in the surface kinetics limited regime. However, the surface kinetics become more important even in the mass transport limited regime as the growth pressure is lowered and mass transport becomes faster. This is due to the increase of the mean time between collisions in the gas phase with decreasing pressure.

2.2 Application of surface kinetics limited growth regime

The surface kinetics limited growth enables fabrication of certain structures, which are difficult to obtain in other growth regimes. For example, lowering the growth temperature and increasing the growth rate shortens

the diffusion length and enables fabrication of InGaAs QWs with higher indium concentration than traditionally [42]. Here the idea of suppressing three dimensional (3D) growth has made it possible to grow high quality InGaAs QWs with high In content enabling luminescence around 1.2 µm as presented in publication VII. For GaInNAs structures it is also essential that growth temperature is maintained low as the desorption of volatile N adatoms from the substrate surface must be suppressed for higher nitrogen incorporation efficiency (publication VII, [43]).

For self-assembled quantum dots the growth is kinetically controlled by surface adatom diffusion [44] and island size and shape can be controlled. The used growth temperatures ($\sim 400 - 550$°C) are low compared to conventional MOVPE temperatures. Increasing growth temperature increases the lateral surface diffusion length causing islands to grow larger reducing the areal island density as shown in Fig. 2.2 (publications II, III).

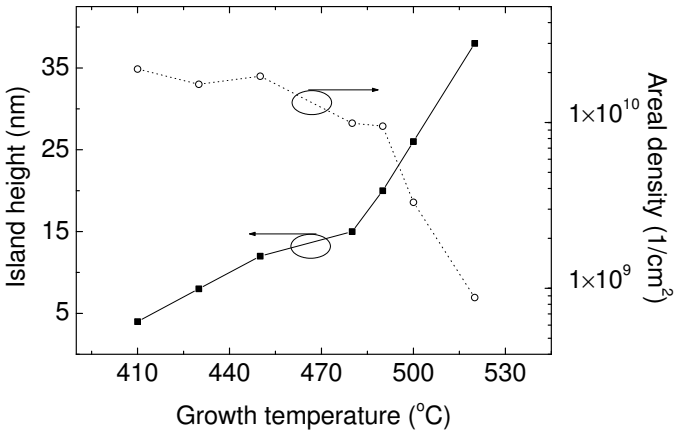

Figure 2.2. Height and areal island density of self-assembled InAs islands directly deposited on Ge substrate as a function of growth temperature. The behaviour is well described by kinetics limited growth. The growth temperatures are thermocouple readings.

On Ge substrate the initial growth phases of a GaAs buffer layer can be controlled via surface kinetics. In publication I high quality GaAs crystals were grown on Ge at low growth temperature of 530°C (all the growth temperatures mention in the overview are thermocouple readings) with very low nominal V/III input ratio of 3.5 utilising the surface kinetics limited growth regime. The GaAs buffer layer growth occurs initially in 3D island nucleation mode, where islands nucleate on the substrate and grow in size until they coalesce. In publication I we showed that lowering the growth

temperature leads to increased island density and so reduces the island size for the coalescence resulting in smoother final surfaces. Chapter 3.3 shows that the reconstruction of the Ge surface is as well temperature dependent. The lower growth temperature also introduces substantial decrease of the undesirable diffusion of As into the Ge substrate.

2.3 MOVPE equipment

Two MOVPE systems shown in Fig. 2.3, installed in the Optoelectronics laboratory of Micronova were used to fabricate the samples presented in this study. Both systems are manufactured by Thomas Swan Scientific Equipment Ltd. The gas distribution system of these two systems is very similar but they differ significantly in their reactor design. The system that was used to grow self-assembled islands of publications II and III has a 1" horizontal reactor and the group III and V input precursors are mixed some centimetres before the halogen lamp heated susceptor tilted a few degrees towards the gas flow. Results in publication I concerning GaAs buffer growth on Ge were carried out in a 3×2" close coupled showerhead (CCS) reactor. Both systems were used for the fabrication of dilute nitride samples. In the CCS design the group III and V precursor flows are brought to the showerhead in separate manifolds and introduced into the reactor from separate microtubes in the showerhead. Substrates are placed on the susceptor some millimetres below the showerhead. The susceptor is heated from below by a resistive tungsten heater. The overall design prevents precursor prereactions effectively and ensures intermixing of different precursors for homogeneous growth. The design also enables comfortable scalability of growth parameters from these small research reactors to high throughput industrial size reactors with possibility to grow several tens of 2" wafers in one growth run.

Fig. 2.4 shows the schematic of the gas distribution system and the reactor layout of the Thomas Swan CCS system. The bubblers are situated in temperature stabilised baths. The purified carrier gas flow is adjusted by mass flow controllers (MFC) through the bubblers, which contain the liquid source materials at controlled pressures. The pressures in the bubblers is adjusted by pressure controllers (PC) connected to the vent lines. The carrier gas is saturated with the metalorganic source material and the output flow is again controlled with one or two separate MFCs and possibly with a dilution line if small molar flows of source material are required. The group III and V source materials are directed prior to the growth into the vent lines

Figure 2.3. MOVPE systems supplied by Thomas Swan Scientific Equipment installed in Optoelectronics laboratory, Micronova.

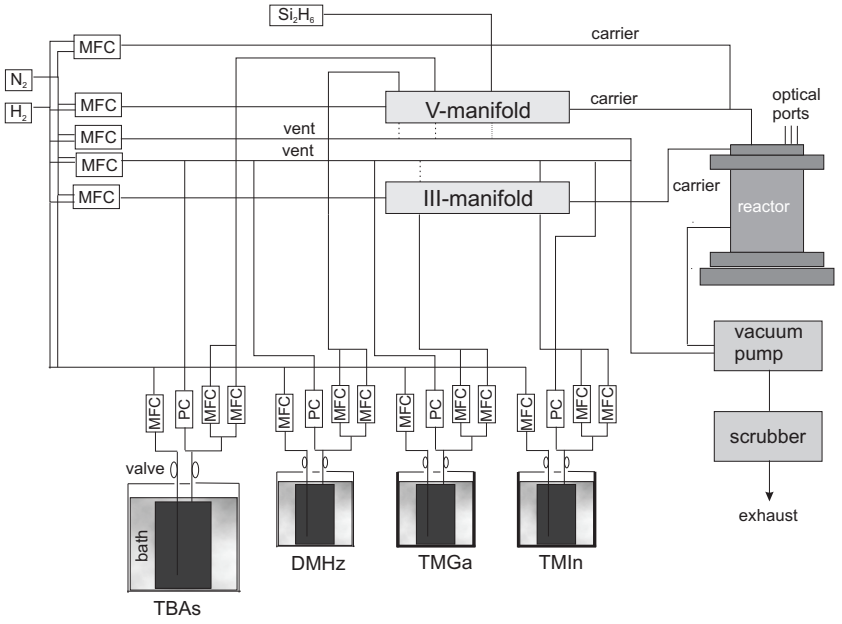

Figure 2.4. Simplified schematic layout of vertical reactor MOVPE system showing the gas distribution system.

to stabilise the precursor flow and switched into the reactor only during the growth of the specified layer. All gas lines are also held at constant pressure independent of the source material flows.

In this study, in addition to the already mentioned TBAs and TMGa, other precursors involved were trimethylindium (TMIn) and 1,1-dimethylhydrazine (DMHz). Disilane (Si_2H_6) gas was used as an n-type dopant source for GaAs. Currently the MOVPE system with 3×2" CCS reactor has also TMAl, TPB, CBr_4 and Cp_2Mg metalorganic sources and NH_3 gas connected.

2.4 Comparison of MOVPE and MBE techniques

Most of the applications on Ge substrates are manufactured using MOVPE technique which is more suitable for commercial production than MBE. MOVPE technique has advantages over MBE such as lower maintenance needs, higher up-time, higher throughput and lower costs. In MBE reactive material atoms and molecules are delivered in separately controlled beams enabling lower growth temperatures and easiness of controlling the growth. Being a high vacuum system, the prereactions and background impurities are a smaller concern in the MBE systems than in MOVPE. For the MBE growth of GaAs/Ge heterostructures conflicting initial growth conditions were first presented. During the 1980's Chand *et al.* reported that As_2 exposed surfaces lead to smooth APD-free GaAs [15]. During the 1990's it was reported that a Ga monolayer prevents the formation of a high step density surface producing good surface morphology for gas-source MBE-grown GaAs layers on Ge [34]. It was also reported that an As_4 flux preserves double step structure providing APD-free growth of GaAs for the solid-source MBE [36]. In 2001 W. Li *et al.* concluded for both SSMBE and for GSMBE that initial exposure to either cracked arsine or As_2 was crucial to obtain APD free growth of GaAs on Ge [37]. Promising results have been produced by low temperature migration enhanced MBE, where As and Ga atom fluxes are in turns switched to the substrate [35, 37]. However, up to date the possibility in MOVPE growth to introduce high partial As pressure in relatively high reactor pressure favours MOVPE technique over MBE for GaAs on Ge heteroepitaxy.

3 Interfacial phenomena

In this chapter the reconstruction of Ge surface and nucleation theories of polar-on-nonpolar semiconductor from several results and publications is presented. The effects of initial growth conditions are studied via diverse self-assembled islands deposited on germanium substrates inspected by atomic force microscope. Also island formation on Ge and GaAs substrate is compared. Finally, a general view into formation of high-quality GaAs buffer layer is illustrated.

3.1 Nucleation morphology

Surface morphology of the samples was probed with NanoScope E atomic force microscope (AFM) presented in Fig. 3.1. The sample was positioned in close vicinity of Si_3N_4 probe tip at the end of flexible cantilever. The cantilever is affected by the van der Waals and Coulomb forces between the sample surface and the probe tip. The sample is moved in lateral direction to perform an image scan. The images of islands were probed using the AFM in a contact mode, where piezo electronics moves the sample also in the vertical direction to maintain the differential of the two different detector output values at zero. The vertical movement gives the actual height information of the scan. The operating principle is schematically showed in Fig. 3.2. The antiphase boundaries of GaAs buffer layers reaching the sample surface were more clearly detected using the AFM in deflection mode were a derivative value of height information is gained. In the deflection mode only the differential signal is measured and converted as height information.

The growth of self-assembled islands was studied by depositing InAs and nominally $In_{0.5}Ga_{0.5}As$ material directly on a Ge surface. Numerous studies concerning In(Ga)As QDs on GaAs substrates have been reported, few rel-

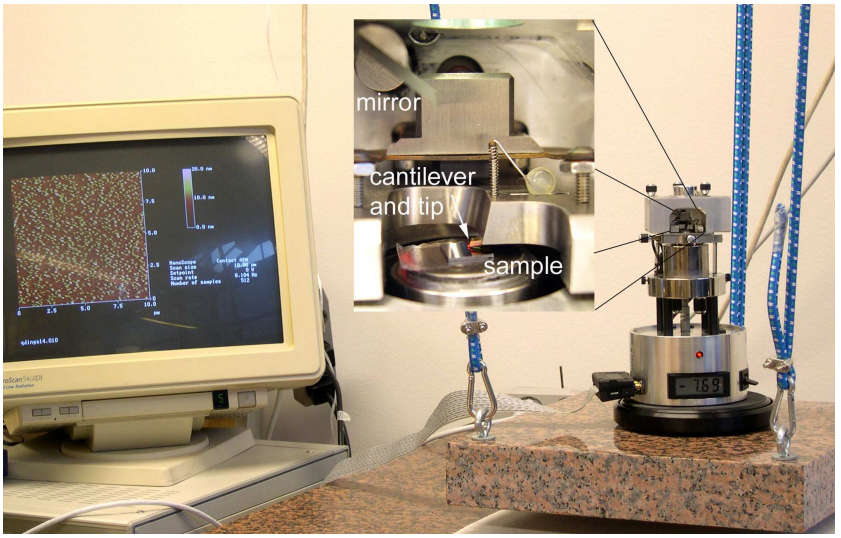

Figure 3.1. Atomic force microscopy Nanoscope E from Veeco installed in Optoelectronics laboratory, Micronova.

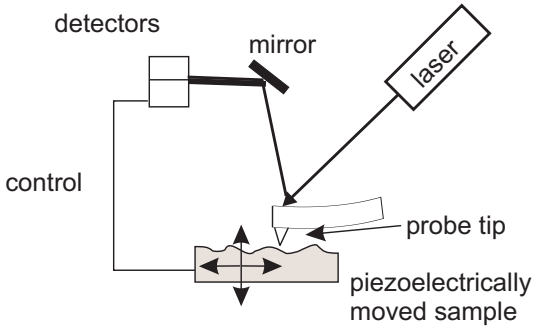

Figure 3.2. Generic layout and operating principle of AFM.

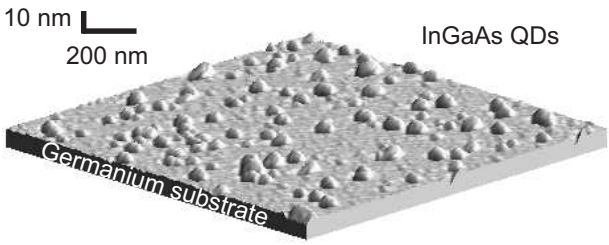

Figure 3.3. Three-dimensional view of nominally 2 monolayers of $In_{0.5}Ga_{0.5}As$ deposited directly on Ge at 550°C forming self-assembled islands. The bars on top left present vertical and horizontal scales of the AFM scan.

evant ones using MOVPE [45–49] and MBE [44, 50–57] can be pointed out. Fig. 3.3 shows an example of 2 monolayers of $In_{0.5}Ga_{0.5}As$ deposited on Ge forming three-dimensional islands. The deposition thickness of compound semiconductors here is presented in terms of the equivalent monolayer coverage for layer-by-layer growth, where a monolayer corresponds to a half of the lattice constant of the grown epitaxial material.

The size, height and density of formed islands as function of growth temperature and coverage were investigated (publication II) and compared to similar growth sequences on GaAs material in publication III. The density of both the InAs and $In_{0.5}Ga_{0.5}As$ islands was found to behave almost identically on both surfaces. However, the initial island formation and the average size and height of the islands were found to differ severely between Ge and GaAs substrates as shown for $In_{0.5}Ga_{0.5}As$ islands in Fig. 3.4.

At low temperature of 550°C $In_{0.5}Ga_{0.5}As$ growth on GaAs appears in the Stranski-Krastanow (SK) growth mode, where an uniform two-dimensional layer-by-layer growth up to the critical thickness is followed by a three-dimensional island growth [44]. The same SK growth mode applies to InAs islands on GaAs [50, 51] but lower growth temperature can be used as this enhances the island density and homogeneity [44]. Surface free energy of $InAs/In_{0.5}Ga_{0.5}As$ is lower than that of GaAs and the epitaxial layer wets the GaAs surface. Driving force for the three-dimensional growth is the lattice mismatch between $InAs/In_{0.5}Ga_{0.5}As$ and GaAs. The epitaxial film grows as strained and as the strain energy builds up, the relation between the surface energy and the strain energy eventually causes the film to undergo an elastic deformation to form 3D island growth. In publication III for $In_{0.5}Ga_{0.5}As$ on GaAs this occurred at coverages above 3.5 ML as indicated in Fig. 3.4. For the InAs islands the critical thickness is reported

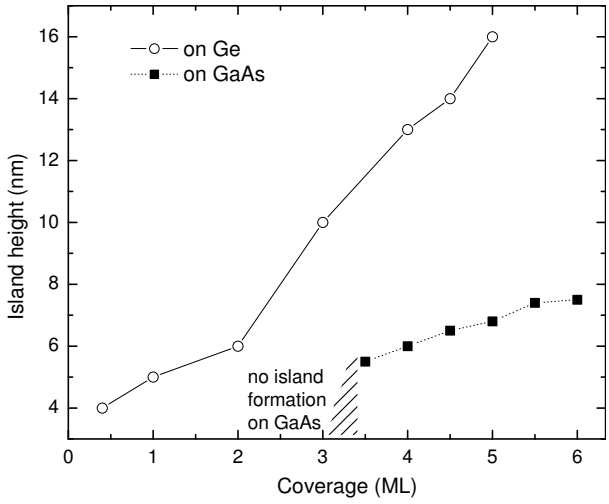

Figure 3.4. Formation of $In_{0.5}Ga_{0.5}As$ self-assembled islands on both Ge and GaAs substrates. Average island height as a function of deposition thickness is presented for islands grown at 550°C with V/III ratio of 10. Due to the development of two-dimensional wetting layer no island formation is detected on GaAs for deposition of less than 3.5 monolayers.

to be about 1.5 ML [58]. The reduction in critical thickness for InAs as compared to InGaAs is because of the increased epitaxial mismatch. The formed In(Ga)As islands can be dislocation-free and the lattice mismatch is entirely accommodated by an elastic distortion, thereby the growth mode is called coherent Stranski-Krastanow growth.

Fig. 3.4 shows that when $In_{0.5}Ga_{0.5}As$ is deposited on Ge the formation of three-dimensional islands occurs already at submonolayer thicknesses. In this Volmer-Weber growth mode the added material can minimise its free energy by trading increased surface area for decreased interface area, i.e., forming 3D islands. In publications II and III the submonolayer formation of islands was observed both for InAs and $In_{0.5}Ga_{0.5}As$ materials on Ge. Fig. 2.2 of chapter 2.2 shows that the InAs island density has exponential dependency on temperature. At increased growth temperatures the decrease in the island density is due to the adatom surface diffusion lengths as the increased lateral and vertical diffusion lengths cause islands to grow higher and larger in diameter [44]. Fig. 3.5 shows top view AFM images of $In_{0.5}Ga_{0.5}As$ on Ge with different 0.4, 1.0, and 4.0 ML coverage. A very low density of islands is already seen for the 0.4 ML deposition indicating

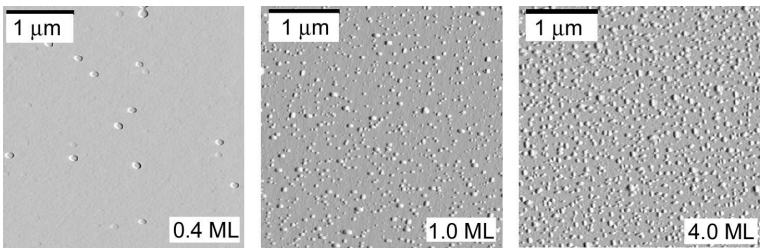

Figure 3.5. Top view AFM images of $In_{0.5}Ga_{0.5}As$ islands on Ge with different deposition thicknesses indicated in the images. The horizontal scale is presented by bars and the full height scale is about 50 nm.

that no two-dimensional wetting layer is formed but the material starts to form directly three-dimensional islands. In publication III the island density was found to increase super-linearly as function of deposition thickness for less than 3 ML coverage. However, the growth temperature remains as dominating tool for controlling the island density. After 3 ML coverage the island density saturates and due to the island coalescence the density starts to decrease after 4.5 ML coverage. Very high density over 10^{10} cm^{-2} with uniform island size of both InAs and $In_{0.5}Ga_{0.5}As$ islands on Ge was achieved at the growth temperatures of 450°C and 550°C, respectively.

3.2 Initial growth phases of GaAs

Regardless of the fact that GaAs on Ge has a very small lattice mismatch of -7×10^{-4}, the nucleation and growth of GaAs is observed to occur by the formation of islands with faceted boundaries [17, 30–32]. Similar behaviour has been obtained for GaAs on Si [6–8] and GaP on Si [11, 59, 60] material systems. In publication I GaAs layers were deposited on Ge substrates both in kinetics and mass transport limited growth regimes. The nucleation mechanism was studied by depositing fairly thin ($\sim$ 20 ML) layers of GaAs on Ge at different growth temperatures. After the growth the surface morphology was characterised using AFM. From Fig. 3.6 it can be verified that the initial growth appears in 3D mode for the GaAs epitaxy on Ge substrates. However, distinctions in the nucleation process are evident for different growth temperatures.

As more GaAs is deposited, the islands grow in size until they touch each other and form a two-dimensional epitaxial layer. For this coalescence process the island density and size distribution are crucial parameters. The optimisation of coalescence process is extremely important to provide high-quality buffer layer for the device growth. When two islands coalesce there may remain a grain boundary between them or they may form a boundary-free area. Surface energies are the factors that control this process through material transport by surface and bulk diffusion. At low, kinetics-limited growth temperatures ($\sim$ 530°C, Fig. 3.6a) the surface diffusion enhances the island density and the coalescence of the islands takes place at smaller and likely more uniform size. This controlling of coalescence enables formation of smooth mirror-like two-dimensional surface as the growth is further carried on. If the growth temperature is raised ($\sim$ 620°C, Fig. 3.6b) the 3D growth mechanism is maintained confirming that the 2D growth actually represents the equilibrium situation rather than being kinetic limitation. However, the island density is reduced inducing the coalescence of the larger and inhomogeneous islands. At high temperatures ($\sim$ 700°C, Fig. 3.6c) the nucleation of GaAs is converted to form hut clusters. S. Onozawa *et al.* discovered these small stick like clusters for GaAs grown on Si in 1988 [10] and Y. Mo *et al.* named them as huts in 1990 when they studied the transition from 2D to 3D growth of Ge deposited on Si substrates using scanning tunnelling microscopy (STM) [61, 62]. These huts are believed to be metastable, an intermediate step towards formation of larger clusters. In publication I they were found to have their principle axes strictly along two orthogonal $\langle 100 \rangle$ directions and rough final surface morphology was found when deposition time was increased.

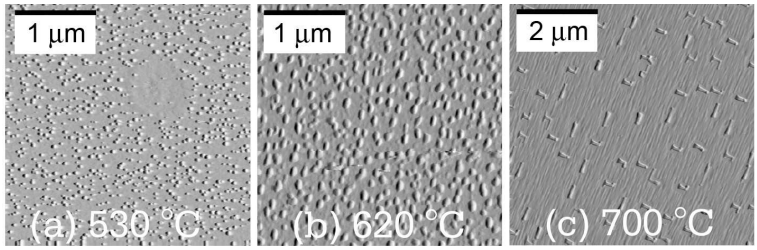

Figure 3.6. Nucleation and initial growth phases of GaAs on Ge at various growth temperatures. For (a) and for (b, c) the V/III ratio was 3.5 and 60, respectively. The horizontal scale is presented by bars in the images and the height scale is 30 nm for the (a) and 50 nm for the (b, c).

3.3 Ge surface reconstruction and morphology of GaAs layers

L. Bobb *et al.* already suggested during 1960's that the epitaxy of polar zinc blende lattice onto non-polar diamond lattice structure can result in two orientations in which the As and Ga sublattices are exchanged, i.e. the GaAs crystals have a 90° rotation about a [001] axis in contrast with each other as shown in Fig. 3.7 [63].

Mostly during late 1980's and 1990's several groups presented somewhat different nucleation models for GaAs on Si and on Ge based on difference in growth temperature, As partial pressure, initial exposure to Ga or As flux and misorientation of the substrate [21, 33, 64–69]. Both Y. Li *et al.* and S. Ting *et al.* presented two different nucleation models, that were based on experiments performed in atmospheric pressure MOVPE reactor for GaAs on Ge. In 1994 Y. Li *et al.* introduced a model where sublattice orientation of polar GaAs material grown on nonpolar Ge material is defined by the relative amount of nucleation at the steps and on terraces between the steps [21]. The two possible sublattice orientations are presented in Fig 3.8 when grown on a (100)-oriented Ge substrate. Y. Li *et al.* assumed that if GaAs initially nucleated at surface steps the sublattice orientation follows GaAs-A

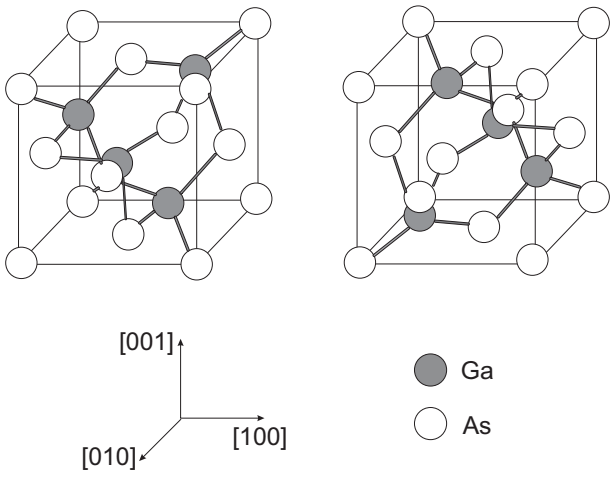

Figure 3.7. Two possible orientations of the GaAs with zinc blende structure. The GaAs crystals have different orientation corresponding 90° rotation about a [001] axis.

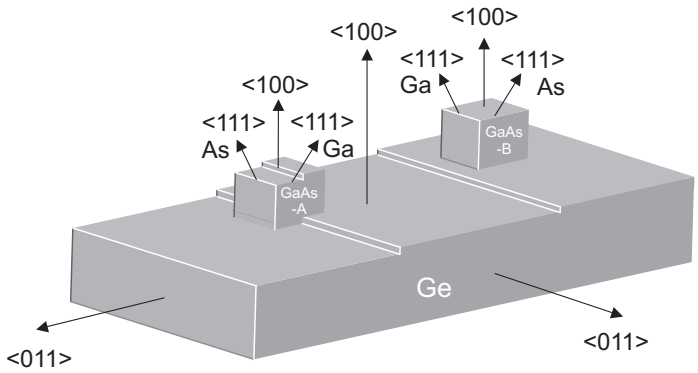

Figure 3.8. Two orientations of GaAs sublattices on Ge. The dominant orientation is defined by kinetics and energetics effects.

and if it initially nucleated at the surface terraces the sublattice orientation follows GaAs-B as presented in Fig 3.8. It was stated that subsequent large misorientation angle can suppress the formation of APDs completely. Y. Li *et al.* also presented model how APBs self-annihilate due to the overgrowth of dominating sublattice orientation for the substrates with small misorientation angles [22–24]. However, no mechanism was presented to explain why nucleation would occur differently on the surface terraces and on the steps.

In 2000 S. Ting *et al.* presented a model based on dimer orientations and their temperature dependence on MOVPE grown GaAs on Ge(100) surface. The model based on several earlier studies and results presented by several research groups [65, 68, 70–72]. S. Ting *et al.* performed the experiments using a MOVPE reactor but were also able to compare the gained results and models with their earlier studies using MBE system. In MBE there are powerful monitoring systems such as reflection high-energy electron diffraction (RHEED) and low energy electron diffraction (LEED), which are essential tools when determining the nucleation and early growth phases in situ. Several studies show that on reconstructed Ge surfaces the arsenic atoms readily adsorb and dimerise in the place of substrate atoms [65, 68]. The resulting arsenic passivated surface is inert and self-limited to one ML coverage. Based on these results GaAs on Ge nucleation can be represented as additive and displacive dimerisation model. In additive dimerisation the As-As dimer orientation becomes perpendicular to the step edges on the Ge substrate. In displacive dimerisation the As-As dimers are oriented paral-

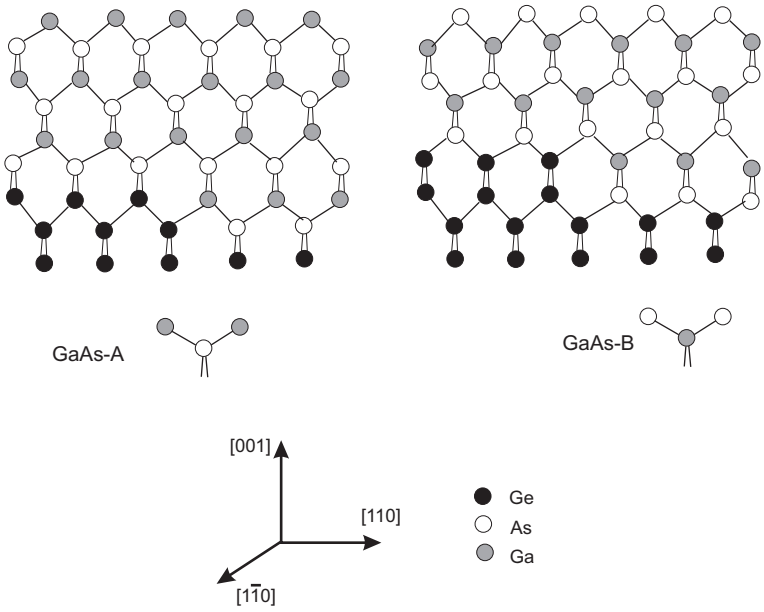

Figure 3.9. Arsenic dimer rotation on double step Ge surface via atomic arrangements. GaAs-A corresponds to perpendicular As-As dimer orientation to step edges (i.e. additive dimerisation) and GaAs-B corresponds to parallel As-As dimer orientation to step edges (i.e. displacive dimerisation).

lel to the step edges. The different bonding of As into Ge and change in the polarity for GaAs sublattice is presented in Fig. 3.9. In the displacive dimerisation the As-As-dimers have displaced the first monolayer of Ge and in the additive dimerisation no modification to the Ge surface has occurred when As-As-dimers are nucleated on the surface. R. Bringans *et al.* reported for GaAs on Si that different dimerisations are selected by kinetic and energetic effects [68]. The lowest energy structure would be displacive dimerisation, i.e., parallel dimer orientation to step edges, but in several cases, the kinetically limited additive dimerisation, i.e., perpendicular dimer orientation to step edges is dominate. Kinetics limitations do not enable long enough presence of As atoms at the step edges to exchange with Ge atoms leading to additive dimerisation.

S. Ting *et al.* showed using MOVPE growth that at high temperatures ($> 600°$C) the annealed Ge surface reconstruction prefers additive dimerisation, and at low temperature the preference shifts to favour of displacive dimerisation. S. Ting *et al.* performed a high temperature annealing of

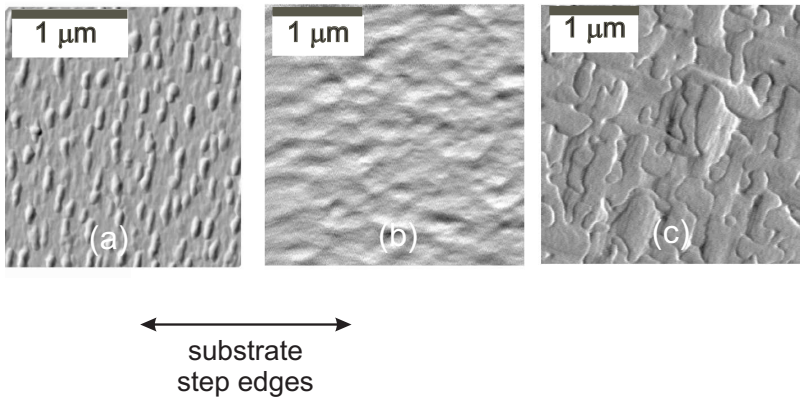

Figure 3.10. Different GaAs surface morphologies on Ge. (a) High temperature growth (above 620°C) showing elongated islands in the perpendicular direction of atomic steps on Ge indicating GaAs-A growth. (b) Low temperature growth (530°C) showing elongated hillocks in the parallel direction indicating GaAs-B growth. (c) Antiphase boundaries reaching GaAs surface due to the use of non-misoriented Ge substrate introducing single steps.

the Ge substrates, prior the growth, in N_2 at 650°C and concluded that the background arsenic pressure in the reactor is suspected to be responsible for the competing mechanism of additive and displacive dimerisations on the Ge surface. However, in publication I the annealing of the substrates, prior to the growth, in H_2 at low 400°C temperature was performed and similar behaviour to R. Bringans results was found. In publication I the AFM studies of initial nucleation showed elongated islands in the perpendicular direction to the step edges indicating additive dimerisation for layers deposited above 620°C as shown in Fig. 3.10a. For the low temperature growth (530°C) no elongated island growth was observed likely because the island density was very high. However, few tens of nanometres thick GaAs layer deposited at low temperature showed hillocks oriented in parallel direction to the step edges as showed in Fig. 3.10b. This indicates displacive dimerisation for low growth temperatures as expected. From these results it is concluded that high temperature annealing, prior the growth, is not necessary to have surface reconstruction on Ge.

However, to have consistent As-As dimerisation on the surface is not enough to produce antiphase boundary free crystal. The height of the surface steps on the substrate must be equivalent to even number (double) to have the same atom on opposite sides of the step. R. Kaplan *et al.* [73], P. Pukite *et al.* [70] and J. Griffit *et al.* [71] stated that the step structure of Si and Ge substrates is formed by two monolayer steps (here monolayer is equivalent to 1/4 of the lattice constant of Ge or Si) and smooth terraces between them when the substrate is misorientated towards [011]. Noteworthy is that for the substrates oriented exactly towards the [010] no dominant step height could be determined. When grown on single step substrate the growth proceeds forming antiphase domains, which are brought together by APBs consisting of Ga-Ga and As-As bonds. APBs are found to be electrically active defects and known to cause carrier scattering and nonradiative recombination [9, 65]. In Fig. 3.11 two differently oriented APBs are presented. An APB is formed if nucleation on Ge starts for one site from Ga and for the other site at the same step from As. Also if nucleation starts from equivalent atom but there exists a odd step height on the substrate between them APB is formed. Formation of such APBs is indicated in Fig. 3.11a. In such cases there exists an equal number of Ga-Ga bonds and As-As bonds resulting in compensated structure. However, in Fig. 3.11b formation of an APB with localised As-As bonds is demonstrated, which self-annihilates but results in donor-like behaviour.

An example of APBs on the surface of GaAs layer grown on a nonmisoriented Ge substrate is presented in Fig. 3.10c, where clear boundaries are present. The APBs reach out trough the epitaxial layer to the sample surface. The APBs are likely to form because a single step structure is expected as the substrate has no misorientation. Due to the low growth rate the surface is quite smooth and the area of APDs is quite large, hundreds of nanometers in width. In addition to the substrate misorientation several other methods such as high group V partial pressure, low growth rate and high growth temperature are presented to lower the APBs density of polar-to-nonpolar epitaxy [17, 23, 74]. However, in publication I smooth surface morphology GaAs layers were grown at low temperature of 530°C with very low group V partial pressure introducing V/III input ratio of 3.5. Later also smooth surface morphology layers have been grown at 575°C with also small group V partial pressure. However, it was noticed in publication I that at growth temperatures above 620°C it is essential to have high partial pressure introducing V/III ratio over 60 to achieve good surface morphology. As it was stated that the surface dimerisation is changed around $\sim$ 600°C the effect of partial As pressure to the surface morphology for different dimer orientations is possible.

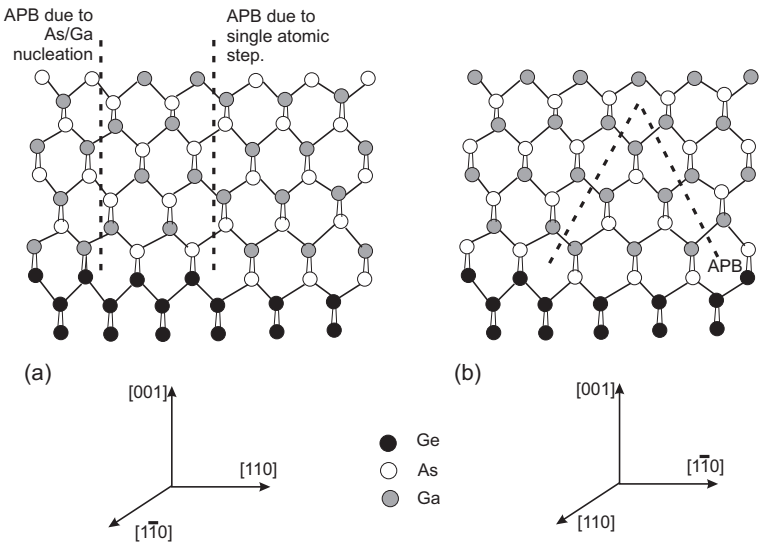

Figure 3.11. Formation of APBs (a) via adjacent nucleation of Ga and As atoms and via single step on the substrate. (b) Single steps introducing self annihilating antiphase boundary.

In conclusion, to form high quality interface between GaAs and Ge it is essential prior to the growth to have reconstruction on the Ge surface with either dominant displacive or additive dimerisation. To form single-domain surface also a double step configuration on the surface of the substrate is necessary. The reconstruction in MOVPE is mainly controlled via temperature and double step formation via the misorientation of the substrate. The misorientation exactly towards [010] is not allowed but should be, for instance, towards [011]. The nucleation and initial growth affect mainly the density and size of the coalesce of islands. Growth parameters that increase the nucleated island density and reduce the size prior to the coalescence should be favoured. The eventual growth parameters and methods depend on whether the end application is, for example, a solar cell, a detector or a light emitting device.

4 Crystal properties and defects

4.1 Characterisation of tilted structures by X-ray diffraction

H. Nagai showed that heteroepitaxy on misoriented substrates results in a tilt angle α between (100) lattice planes of the epitaxial layer and the substrate [75]. The magnitude of the tilt is related to lattice constant separation and misorientation angle via $\tan\alpha = (\tan\varepsilon)\Delta d/d_s$. Where ε is the misorientation of the substrate, i.e., the angle between the Ge substrate surface and the Ge (100) lattice planes and Δd is the lattice parameter difference in the growth direction of the epitaxial layer (d_e) and substrate (d_s) [75, 76]. The tilt is built up to avoid formation of lattice defects at step interfaces as illustrated in Fig. 4.1. The misorientation of the substrate increases the step density as terrace widths are decreased and results in larger tilt between the lattice planes. Correspondingly the relative difference between the lattice constants determines the step height separation between the substrate and the layer. In publication I X-ray diffraction was used to study tilt values of GaAs layers grown on misoriented Ge.

High resolution X-ray diffraction (HRXRD) is an effective method to study crystal quality, epitaxial composition, layer thicknesses, and relaxations of semiconductors. X-rays, having the photon energy of about 8 keV, penetrate into the sample a depth of max 10 µm. The technique is a non-destructive, fast method to characterise the lattice structure. Fig 4.2 shows an photograph of the X-ray diffraction equipment used in this study. A schematic layout of the high-resolution diffractometer with optics and specified angles is illustrated in Fig. 4.3.

In the X-ray diffractometer only the Cu $K_{\alpha 1}$ (1.540553 Å) wavelength is passed through a four-crystal Ge (220) monochromator [77]. The highly parallel and monochromatic beam enters the sample at an angle ω, and

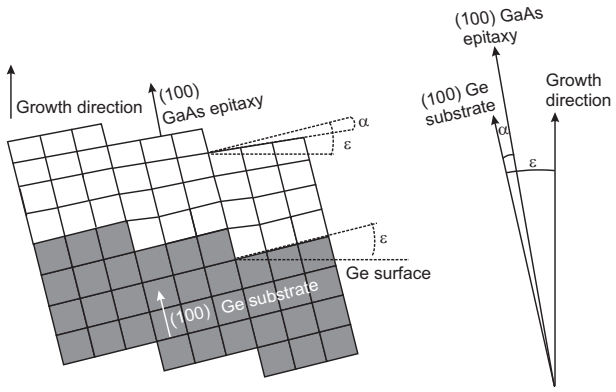

Figure 4.1. Formation of negative tilt of a GaAs epitaxial layer grown on a misoriented Ge substrate. The surface normals are described by arrows. The misorientation ε and the tilt angle α compared to the growth direction are presented.

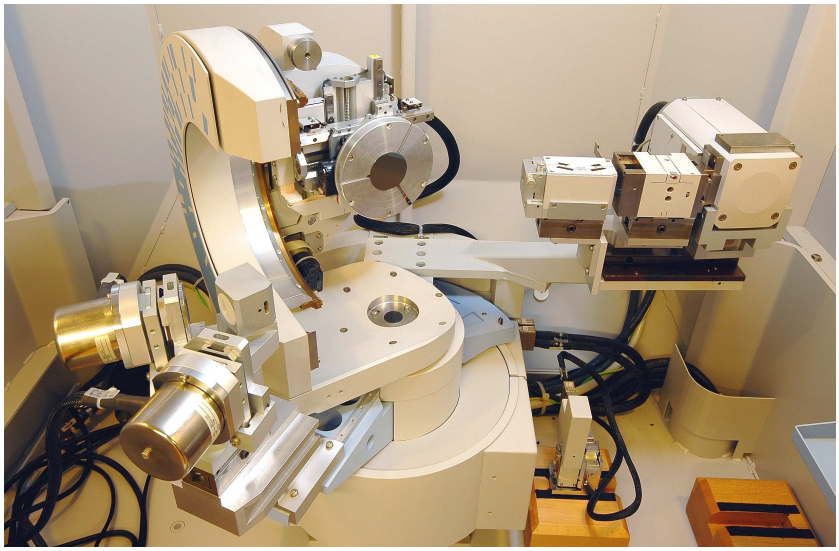

Figure 4.2. Inside view of PANanalytic's X'Pert PRO MRD high resolution X-ray diffraction system installed in Optoelectronics laboratory, Micronova.

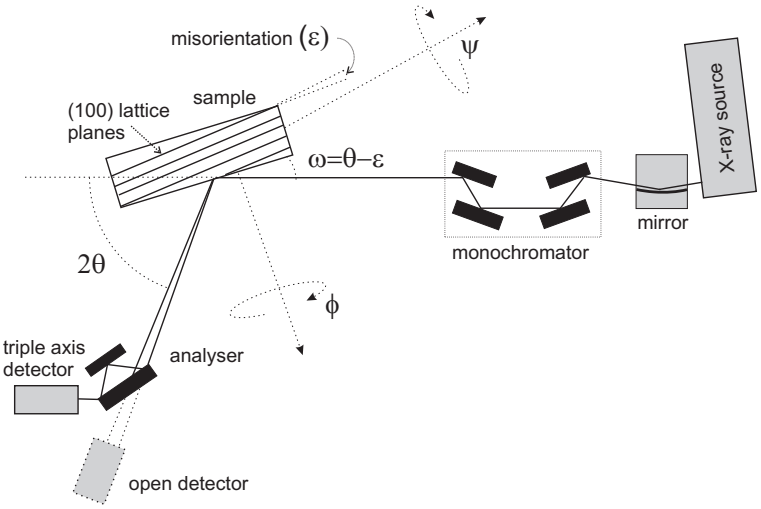

Figure 4.3. Schematic layout of high resolution X-ray diffraction equipment including relevant components and adjustable angles. The diffraction plane is coincident with the paper surface.

the Bragg diffraction angle θ depends on the spacing between the lattice planes. In a two-axis setup the signal is detected with an open detector using a large acceptance angle of about 1° for 2θ. However, because of the large acceptance angle, the open detector is unable to separate diffuse scattering or small composition deviations. By using an analyser crystal in front of the detector, the acceptance angle can be reduced to 12 arc seconds for the 2θ angle [77]. This setup, the triple-axis configuration, also increases the signal to noise ratio and enables resolution high enough for the reciprocal space mapping of the samples. Reciprocal, or as presented here, angular space mapping is an effective method to study samples with tilts between the corresponding lattice planes.

When analysing heterostructures the layer thicknesses and compositions can be found by comparing the measured $\omega - 2\theta$ scan to simulated diffraction curves. In the $\omega - 2\theta$ scan both the ω and 2θ are moved so that the relation $\omega = \theta - \varepsilon$ is valid, where ε is the misorientation angle of the substrate. However, if misorientation ε is present in the heterostructure, measuring the $\omega - 2\theta$ diffraction curve is complicated as there very likely is an additional tilt α between the lattice planes of the substrate and the layer. In such a case two different relations $\omega = \theta - \varepsilon$ and $\omega = \theta - \varepsilon - \alpha$ would be true for the substrate and layer, respectively, and therefore no $\omega - 2\theta$ scan could easily be performed simultaneously for the whole structure.

Fig. 4.4 shows a 004 angular space map of a GaAs epitaxial layer grown on a 6° towards ⟨111⟩ misoriented Ge substrate. The scan is performed in the perpendicular setup, where the step edges on the Ge surface are in the direction of a diffraction plane normal (Fig. 4.5). The angular space map reveals a tilt angle α of about 0.007° between the GaAs and Ge (100) lattice planes. The grey horizontal line in the figure illustrates the situation where a single $\omega - 2\theta$ scan with an analyser crystal would be performed for the structure using the $\omega = \theta - \varepsilon$ relation. As can be seen, no information about the epitaxial layer would be gained. If an open detector would be used, with an $\Delta\omega$ acceptance angle of about 0.5°, the measured $\omega - 2\theta$ curve would result approximately in a projection of the intensity in the angular space map to the x-axis. However, this projection would result in an untrue separation between the substrate and layer peak [78]. H. Nagai studied InGaAs layers deposited on misoriented GaAs substrates and stated that

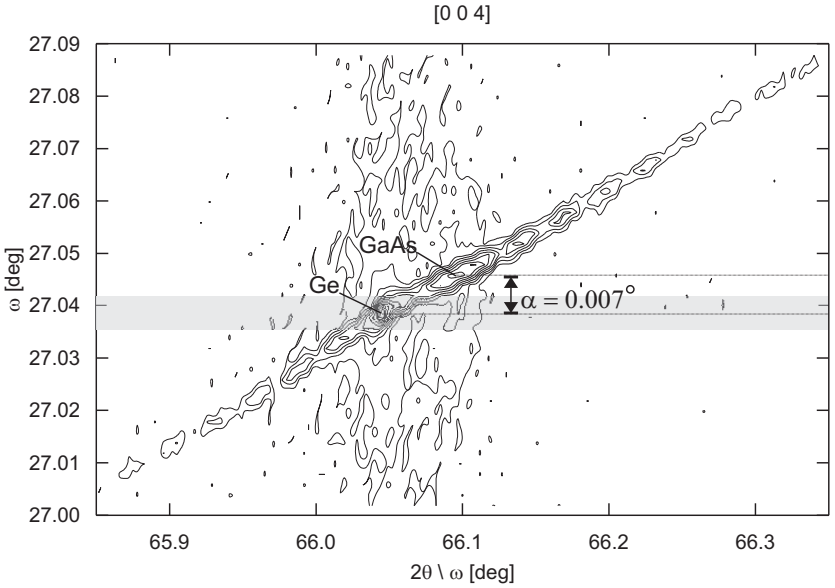

Figure 4.4. 004 HRXRD angular space map of GaAs epitaxial layers on 6° misoriented Ge substrate. The intensity doubles between adjacent contours. The measurement is conducted in the perpendicular setup (i.e. the diffraction plane perpendicular to the step edges). The amount of tilt α is found from the vertical displacement of the Ge and GaAs peaks. The gray line in the figure presents information gained if a single high resolution diffraction scan would be performed in the same alignment.

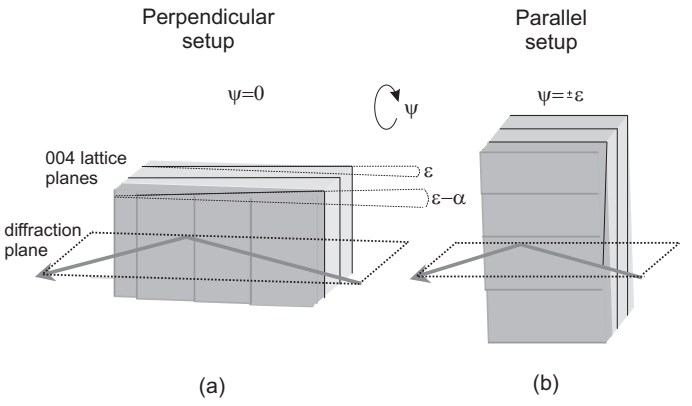

Figure 4.5. High resolution XRD measurement setups. a) In the perpendicular setup (i.e. diffraction plane perpendicular to the step edges) using $\omega = \theta - \varepsilon$ relation. b) In the parallel setup (i.e. diffraction plane parallel to the step edges) using $\omega = \theta$ relation when the (ψ) angle of the sample is rotated to compensate ε. Later alignment enables scans containing information of the whole structure.

the tilt is formed in the direction of the substrate misorientation and is not present for the perpendicular directions, i.e., in the direction of the step edges [75, 79]. In publication I a similar orientation of the α was confirmed for the GaAs/Ge structure. This result enables a single $\omega - 2\theta$ scan in the triple axis setup to display information of the whole structure, provided that the scan is performed in the parallel setup as illustrated in Fig. 4.5. In the parallel setup the diffraction plane lies in the direction of the step edges. The real layer thicknesses and compositions can then be obtained from a simulation. However, to perform such a scan the ψ and ϕ angles of the sample (indicated in the Fig. 4.3) must be rotated according to the amount and direction of the misorientation ε, respectively. In such an alignment the tilt has an minimal effect and results in an insignificant error. Fig. 4.6a shows a 004 angular space map of the same sample as in Fig. 4.4. The scan has been performed in the parallel setup, thus no tilt is observed in the map as expected. In Fig. 4.6b a single 004 $\omega - 2\theta$ diffraction curve scan performed in the parallel alignment and a simulation of 188 nm thick GaAs layer on Ge are shown. The excellent agreement between measured and simulated curves indicates nearly perfect crystal structure and the clarity of the fringes gives evidence of a high-quality interface between the Ge and GaAs materials.

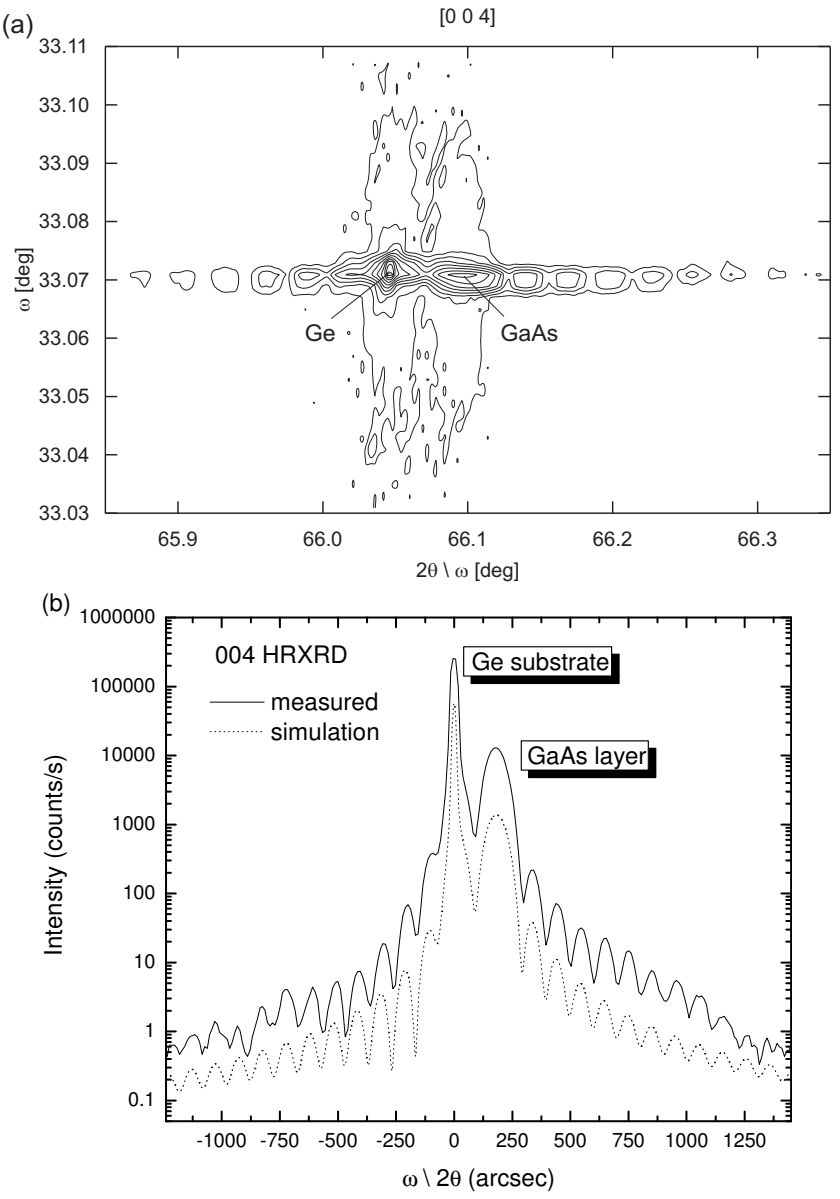

Figure 4.6. (a) 004 HRXRD angular space map of GaAs epitaxial layers on 6° misoriented Ge substrate when the parallel setup (i.e. diffraction plane parallel to the step edges) is used. The intensity doubles between adjacent contours. (b) Corresponding diffraction curve. The dotted line shifted downwards for clarity shows a simulation of 188 nm thick GaAs layer on Ge.

4.2 Analysing defects using synchrotron X-ray topography

Synchrotron X-ray topography (SXT) is used to image individual dislocations and to gain information about other extended defects. With fairly straightforward analyses also the type and the Burgers vector of the dislocations can be solved [80]. The very high intensity and the wide spectrum of synchrotron radiation allow high resolution transmission and back reflection diffraction images of strongly absorbing materials using relatively short exposure times. The topography technique is very sensitive to strain fields generated by different dislocations and even single misfits can be revealed [81]. The topographs in this study were recorded in the Hamburger Synchrotronstrahlungslabor HASYLAB using large-area transmission, large-area back-reflection, section transmission and section back-reflection geometry. Fig. 4.7 shows the schematic layout of the large-area back-reflection topography technique. One incident and few of the numerous diffracted beams are drawn in the figure. Because the germanium substrates can be grown with very good quality, low dislocation and defect densities are enabled in the epitaxial layers. This was proven in publications I and V wherein mixed type threading or circular arc dislocation density of $250-500$ cm^{-2} was determined from the topographs of a 650 nm thick GaAs layer. In contrast to a study by E. Müller no stacking faults were found in the topographs [82]. The most common direction of the dislocations was determined in publication I to be $[\overline{1}\,0\,1]$.

The overall dislocation density of GaAs on Ge is clearly less than what was found in high quality vapour pressure controlled Czochralski (VCz) grown GaAs substrates studied in publication IV showing a typical dislocation density of 1500 cm^{-2}. The strain relaxation mechanism of tensile GaAs on Ge substrates was studied in publication V. Above critical thickness the strain relaxes through misfit dislocations usually formed close to the interface of the mismatched layers [83]. Fig. 4.8 shows a misfit dislocation network of a 750 nm thick GaAs layer on (001) Ge. The number of misfit dislocations is measured from the figure to about 500-600 adjacent dislocations/cm in the directions of $[1\,1\,0]$ and $[1\,\overline{1}\,0]$. For a completely relaxed GaAs/Ge structure the saturation misfit density is calculated to be 3.8×10^5 cm^{-1} [17]. The very small number of misfit dislocations of the 750 nm thick layer and the absence of misfit dislocations in the 650 nm thick layer (in publication I) suggest a critical thickness of about 700 nm for a GaAs/Ge structure grown at low growth temperature of 575°C. This value is above what is conven-

tionally expected for the 0.07 % mismatched GaAs/Ge system. However, because of the lower growth temperature the reduced thermal stress and the formation of tilt via reorientation of the lattice planes are likely to enhance the critical thickness [75, 84, 85]. It is observed from Fig. 4.8 that in the [1 1 0] direction the dislocations are parallel to each other whereas in the [1 $\overline{1}$ 0] direction a small deviation angle exists between adjacent dislocations. This observation agrees with the results of Nijenhuis *et al.*, as they concluded similar behaviour for GaAs layers grown on InGaAs substrates [86]. Nijenhuis *et al.* stated that under tensile stress (as the GaAs/Ge system) a difference in the mobility between As and Ga dislocations can result in a asymmetrical strain relief at low growth temperatures. Formation of misfit dislocations was also studied in publication VI for GaAsN layers grown on GaAs substrates and later for GaAsN/GaAs/Ge systems, from which the results are presented in chapter 5.

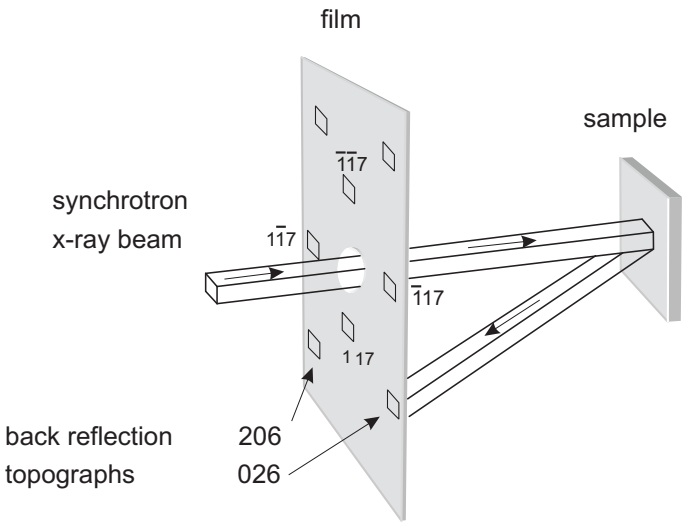

Figure 4.7. Schematic layout of the large area back reflection topography technique, where the synchrotron X-ray radiation hits the sample through a hole in the film and forms several topographs of different lattice planes on the high resolution film.

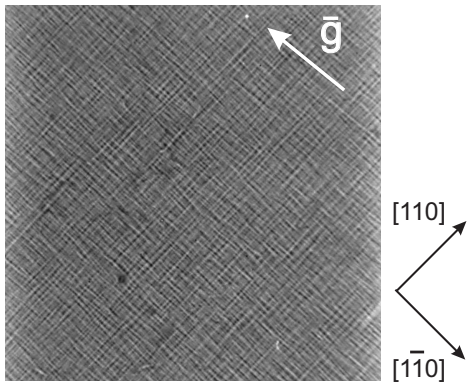

Figure 4.8. 004 large area back reflection topograph of 750 nm thick GaAs epitaxial layer on (001) Ge showing misfit dislocation network. Image size is 1.6×1.6 mm^2 and the diffraction vector **g** projection is marked with an arrow.

4.3 Optical characteristics and interfacial diffusion

In photoluminescence (PL) free carriers are excited into the material by optical excitation. General information on the material quality can be gained as electronic transitions, in particular radiative recombinations of electron-hole pairs, are detected [87]. Several studies on luminescence of GaAs and GaAs/Ge heterostructures have been reported concerning band structure and n-type doping of GaAs as well as different shallow and deep levels in GaAs/Ge structures [88–90, 90–95]. In all studies a dominant peak near the band gap E_g of GaAs (1.519 eV at 0 K and 1.424 eV at room temperature (RT)) can be found related to donor to valence band (VB) transition associated with germanium donor (Ge_{Ga}) centres. In addition, at low temperatures below 77 K following transitions are recognised: around 1.48 eV a conduction band (CB) to germanium acceptor (Ge_{As}) transition [93], around 1.45 eV a Ge_{As} to arsenic vacancy V_{As} transition [91, 94], around 1.41 eV a Ge_{As} to interstitial arsenic atom (As_i) or Ge_{As} to arsenic antisite (As_{Ga}) [94] and a broad lower energy line around 1.2 eV corresponding to V_{Ga} bound to Ge_{Ga} [91]. The 1.2 eV luminescence is noticed only for the n-type samples with the carrier concentration above 1×10^{18} cm^{-3}. Also in this study low energy luminescence was found for the Si doped n-GaAs layers used in the detector structures discussed in chapter 5. In addition, the low energy luminescence could be found from some GaAs layers grown at higher temperatures, above 620°C. This is due to the out-diffusion of Ge into the GaAs layer acting as a donor and introducing n-type doping into

the GaAs layer. The discussed transitions in the GaAs/Ge structures are presented in Fig. 4.9, which shows low temperature (T=9 K) PL spectra of undoped GaAs (T_G = 620°C, V/III = 60, t = 650 nm and n-type GaAs (T_G = 620°C, V/III = 60, t = 250 nm, n = 6×10^{18} cm^{-3}) layers grown on Ge. The broadening of the luminescence spectrum with heavy n-type doping is due to the band-filling of the CB and bandtailing as n-GaAs layer becomes degenerate [96–98]. The out-diffusion of Ge into GaAs was also observed in the secondary ion mass spectrometry studies in publication I, though the diffusion of As into Ge was found to be more significant. It was stated in publication I that two different diffusion mechanisms are responsible for the As diffusion into high-purity Ge: i) the concentration independent diffusion of As related to interstitial sites was found to cause high As concentration close to the GaAs/Ge interface and ii) the concentration dependent diffusion related to vacancies was found to extend deeper into Ge showing lower As concentration [99].

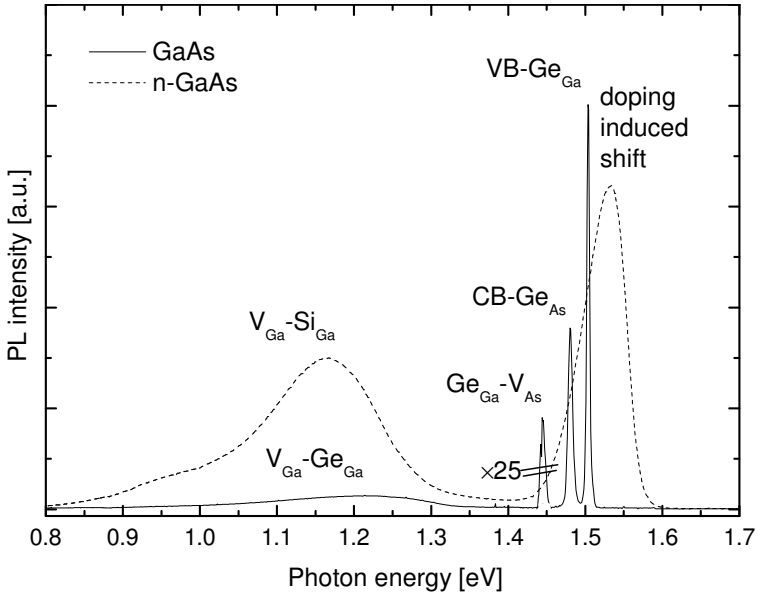

Figure 4.9. Low temperature (T=9 K) photoluminescence from an undoped GaAs layer on Ge and from a Si doped n-GaAs layer on Ge. The different transitions due to the impurities are identified. The peak around 1.45 eV of the undoped GaAs layer has been multiplied by 25 for clarity.

5 Applications

The germanium substrates have several applications in micro- and optoelectronics. GaInP/Ga(In)As/Ge three-junction solar cells with conversion efficiency around 31 % under space-solar spectrum (AM0, 1-sun) are among the most important applications currently in production [100–102]. Prior to the three-junction solar cells in early 1990's several scientific groups studied single-junction cells based on the GaAs/Ge structure [19, 103, 104]. After Weyers *et al.* [105] discovered the large band gap bowing effect of GaAsN and Kondow *et al.* [106] introduced a novel GaInNAs compound, several propositions and studies of multi-junction solar cells were presented on both GaAs and Ge substrates [107–110]. However, the difficulty of short minority-carrier diffusion lengths in GaInNAs must still be overcome to gain high, over 40 %, conversion efficiencies [111]. Light emitting diodes (LEDs), laser diodes and micro cavity LEDs on germanium have also been demonstrated [112–114]. The results are well comparable and close to those from the GaAs-based components, despite the fact that relatively little effort have been placed into the research of light emitting components on Ge. However, expeditiously growing LED based lighting technology including traffic lights and tail lights for cars etc. demand lower costs. Ge provides a small strain reduction for the GaInNAs structures. The strain reduction using intermediate layers is found to improve the optical quality of dilute nitride materials [115]. Also Ge has higher thermal conductivity than GaAs and enables more efficient cooling. However, the rather small band gap of Ge prevents bottom-emitting solutions for wavelengths below 1.88 µm fabricated on Ge which is transparent material only at longer wavelengths. Also high performance InAs Hall sensors have been epitaxially manufactured on Ge [116]. In radiation detectors Ge is widely used because of its advantageous physical properties. The detector applications are more closely presented in chapter 5.1. In chapter 5.2 dilute nitride GaAsN layers and GaInNAs quantum well structures grown on Ge having luminescence on telecommunication wavelengths are introduced.

5.1 Radiation detectors

In radiation detectors germanium is used as an intrinsic (i) region. Under reverse bias an electric field is used to deplete the i-region. Arriving photons interact with Ge producing electrons and holes. The charge carriers are transported to the n- and p-electrodes and converted into a signal. The germanium detectors are particularly sensitive to high energy, i.e., short wavelength radiation such as X-rays and gamma rays. Germanium is available with very high crystal quality with a zero etch pit density (EPD) and a very low impurity concentration of the order of about 10^{10} cm^{-3}. This enables long carrier lifetimes and full depletion with low bias voltages. Also good energy resolution can be obtained as Ge has low electron-hole pair creation energy due to the relative low band gap of 0.66 eV. High-purity germanium is grown by the Czoralski-technique where the impurity concentration is controlled via dislocation density. Too small a dislocation density (less than 100 cm^{-2}) can hinder the annihilation of excess vacancies during the cooling after solidification and leads to hole trapping centres. Too large a dislocation density (more than 10000 cm^{-2}) leads to charge trapping by dislocations themselves. This is the reason that a higher dislocation density is often found in high-purity Ge substrates than in conventional ones. In radiation imaging often high-spatial resolution is required but conventional germanium fabrication processes do not enable finely segmented structures [117]. A GaAs layer on Ge as an n- or p-type contact would enable these finely segmented detector matrixes to be fabricated by patterning the GaAs layers. Separate p- and n-type GaAs layers could be grown in the opposite sides of the Ge wafer to form a p-i-n structure. The electrical properties of the Ge-GaAs heterojunctions were already studied in early 1960's by R. Anderson by growing Ge on GaAs substrates [118]. Later S. Strite *et al.* have studied the electrical properties of the Ge/GaAs structures by growing Ge layers on GaAs substrates for transistor applications [1] and M. Hudait *et al.* [119] studied MOVPE grown n-GaAs/n-Ge heterojunctions using Au-n-GaAs/n-Ge/Au-Ge/Au Schottky-junctions. Due to the relatively narrow band gap of Ge thermal generation of charge carriers must be limited by cooling the detectors. Liquid nitrogen at the temperature of 77 K is usually suitable to reduce the reverse-leakage current to an acceptable level. In publication VIII current-voltage (I-V) curves from the detector matrixes were measured. N-type GaAs layers doped with Si were grown on Ge wafers and processed into pixel detector structures. The I-V measurements were performed by applying a voltage to the unpatterned bottom side with a Au contact and the pixel and a surrounding guard ring were hold at ground potential. Simultaneously the current from

the pixel was measured. Fig. 5.1 shows the structure and two measurements performed at room and at liquid nitrogen temperatures. At 77 K very low leakage currents of about 10 pA were obtained for a 0.3 mm^2 pixel at reverse bias of 100 V.

However, for the detector structures the diffusion of As into the Ge substrate is problematic. Because very high-purity Ge material is used, the formation of shallow As doped n-type germanium material in the direct vicinity of GaAs/Ge interface is quite unavoidable. In publications I and VIII very similar results concerning As diffusion into Ge were obtained from secondary ion mass spectrometry and from I-V measurements as a function of etching depth of the mesas. Low growth temperature was found to hinder the concentration dependent diffusion effectively reducing the overall diffusion depth. However, concentration independent diffusion element was still found to cause high As concentrations very close to the interface. In our recent experiments arsenic has been appropriately diffused into Ge wafers in the MOVPE reactor and the pixel structures have been manufactured into this As-diffusion doped germanium. The detector resolution is measured to be excellent 220 eV at 5.9 keV and 400 eV at 60 keV.

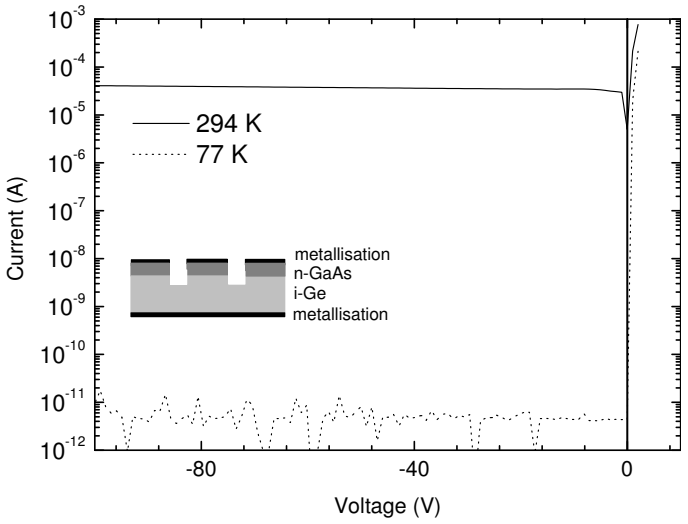

Figure 5.1. Schematic structure and I-V-curve of a GaAs/Ge matrix detector pixel measured at room temperature and at liquid nitrogen temperature.

5.2 GaAs based nitride compounds on Ge

Incorporation of nitrogen into GaAs material affects differently on the physical properties of GaAs than in conventional semiconductor alloys. The unusually strong behaviour of the band gap E_g as the composition of N is altered, know as band gap bowing effect enables telecommunication wavelengths up to 1.55 µm using GaInNAs compounds [105, 106]. The band gap of AB_yC_{1-y} semiconductor compounds is well described by the equation 5.1. For the most semiconductor compounds the band gap change from the AB properties to the AC properties is almost linear and the bowing parameter b is less than 1 eV. However, for the $GaInN_yAs_{1-y}$ compound b is composition dependent and is of the order of 25 eV below y<0.01 and about 16 eV for larger values of y [120–122].

$$E(AB_yC_{1-y}) = (1-y)E_{AC} + yE_{AB} - by(1-y) \tag{5.1}$$

Already a small amount, less than 1 %, of nitrogen causes a large redshift to the band gap, increases the effective electron mass [123, 124] and decreases the electron mobility of GaAs [111]. These anomalous properties of dilute nitride layers are understood through large electronegativity and size differences of As and N atoms. The covalent radii are 0.12 nm and 0.07 nm for As and N, respectively. The larger electronegativity of a nitrogen atom compared to As makes the Ga-N bond more polar favouring electron localisation around the nitrogen atom.

Fig. 5.2 illustrates the band gap vs. the lattice constant of relevant semiconductor materials including GaN compound. Only the variation of E_g for $GaAs_{1-y}N_y$ and $Ga_{1-x}In_xN_yAs_{1-y}$ compounds are shown by bowed lines for clarity. The figure shows that $Ga_{1-x}In_xN_yAs_{1-y}$ material can be grown on Ge substrates lattice matched, compressively strained or tensile strained. However, difficulties arise as the solubility of nitrogen into GaAs based compounds is very limited [105, 125]. The growth of lattice matched layers ($x \approx 3y$) is especially important for solar cell structures on Ge [108, 126] and on GaAs [109], as thick layers are necessary. For long wavelength (1.3 µm) laser components compressively strained $Ga_{1-x}In_xN_yAs_{1-y}$ QW layers with $x \sim 10-35$ % and $y \sim 1-3$ % on GaAs are successfully used [127–131]. In publication VII new approach achieve long wavelengths using dilute nitride QWs on Ge was introduced.

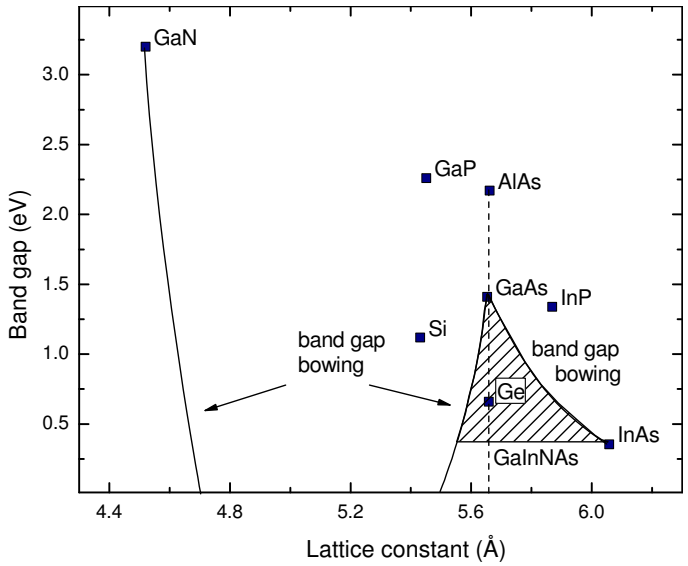

Figure 5.2. Band gap *vs.* lattice constant of relevant III-V compounds including dilute nitride materials and GaN. The strong band gap bowing of nitrogen containing GaAs compounds is shown and patterned area describes possible compounds of $Ga_{1-x}In_xN_yAs_{1-y}$ material.

Several models have been proposed to describe the electronic structure of GaInNAs. In this study a band anticrossing (BAC) model was used to estimate the nitrogen compositions. The BAC model was presented by Shan *et al.* in 1999 and despite its simplicity it can explain III-V-N phenomena successfully [132]. In the BAC model the strong interaction between the conduction band (CB) and a narrow nitrogen introduced resonant band leads to a splitting of the CB into two subbands E_-/E_+ and a reduction of the overall band gap energy. The incorporation of N into InGaAs quantum wells (QWs) on Ge was studied in publication VII and compared to the similar structures grown on GaAs substrates. The results indicated a more efficient solubility of nitrogen into the layers grown on Ge than into those grown on GaAs substrates. Effects of lower surface temperature and strain compensation on Ge were suspected as the major contributions enhancing nitrogen incorporation compared to the structures on GaAs.

Comparison of nitrogen solubility was also recently done for GaAsN layers where the strain compensation is reversed to favour the GaAs substrate but the growth temperature difference remains the same (i.e., likely favours

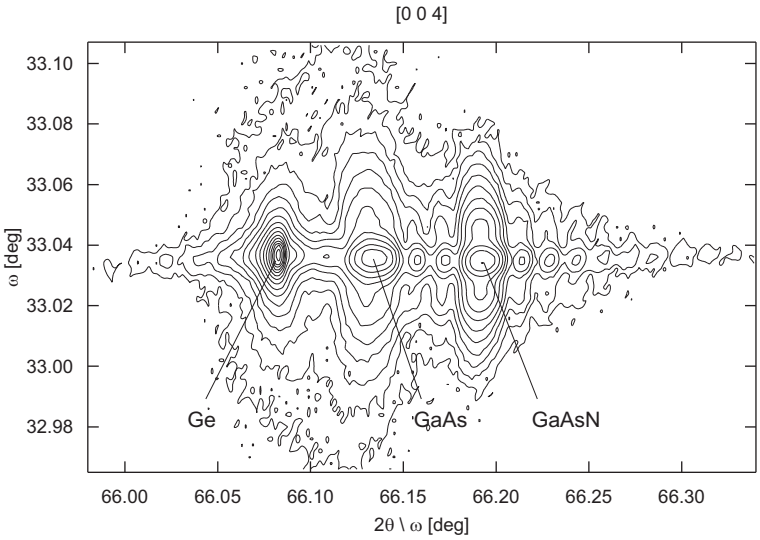

Figure 5.3. 004 angular space map of GaAs-$GaAs_{0.996}N_{0.004}$ structure grown on misoriented Ge substrate measured the step edges parallel to the diffraction plane (i.e. parallel setup). The intensity doubles between adjacent contours.

the Ge substrate). The studies strengthen the previous proposals as no measurable difference of nitrogen incorporation was noticed for the Ge and GaAs substrates. Fig. 5.3 shows a 004 angular space map and Fig. 5.4 shows a 004 $\omega - 2\theta$ diffraction curve of a studied GaAs-GaAsN structure grown on Ge. Both measurements were done in the direction of the step edges ,i.e., parallel X-ray diffraction setup. Fig. 5.4 also shows a 004 $\omega - 2\theta$ diffraction curves of the same structure grown simultaneously on GaAs and a simulation of $GaAs_{0.996}N_{0.004}$/GaAs/Ge structure with layer thicknesses of 364 nm and 285 nm, respectively.

In publication VI creation of misfit dislocations on GaAsN layers as function of the N composition and layer thickness on GaAs substrates was studied. For a 500 nm thick GaAsN layer on GaAs with nitrogen content of 0.9 % few misfit dislocations were detected. However, when grown on Ge similar amount of misfit dislocations were observed for the GaAsN/GaAs/Ge structure with nitrogen content of 0.4 % and GaAsN layer thicknesses of 364 nm. This is due to the additional strain induced both by the Ge substrate and the 285 nm thick GaAs buffer.

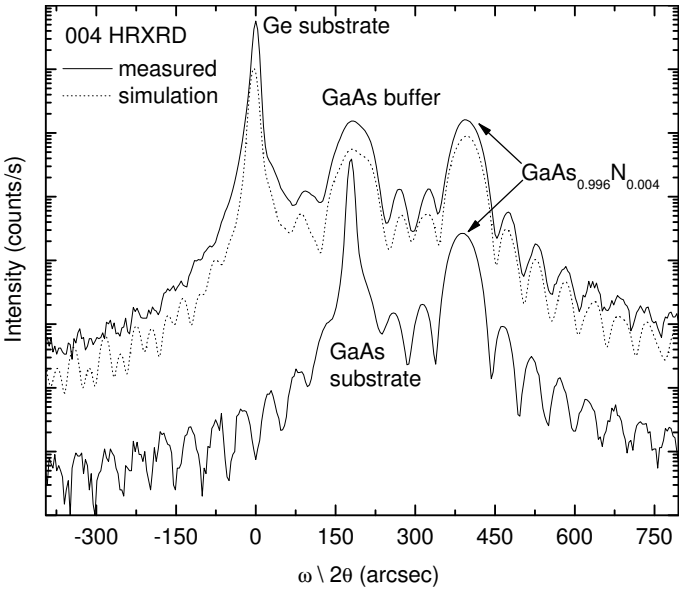

Figure 5.4. Topmost curve shows a 004 HRXRD diffraction curve of the GaAs-GaAsN epitaxial layer on misoriented Ge substrate measured in the parallel setup. The dotted line shifted downwards for clarity shows a simulation of a 285 nm thick GaAs and a 364 nm thick $GaAs_{0.996}N_{0.004}$ layer on Ge. In addition, the lowest curve shows an 004 HRXRD diffraction curve of the structure on a GaAs substrate.

The growth of the GaInNAs QW in publication VII was performed using two MOVPE equipments. A GaAs buffer was grown in the 3×2" vertical CCS reactor and the dilute nitride layers in the horizontal reactor. The following results were completed using the CCS reactor and performed entirely in a single growth run. The growth cycles consist of a 200 nm thick GaAs buffer and $3\times Ga_{0.83}In_{0.17}N_yAs_{1-y}$/GaAs (6 nm/15 nm) QW structure grown at 575°C. The results concerning nitrogen incorporation efficiency favouring Ge over GaAs were well congruent with the results presented in publication VII. Fig. 5.5 shows room temperature PL measurements of the $Ga_{0.83}In_{0.17}N_yAs_{1-y}$ multi-QW structures with different nitrogen contents. Intensities have been scaled to make the figure clearer and the scaling factors are shown below each spectrum. The indium content of the samples was determined from XRD analyses to about 17 %. The spectrum of the InGaAs sample on the right shows the narrowest spectral width but the highest intensity is observed from the nitrogen sample with low nitrogen content. This is due to the larger conduction band offset, which provides a

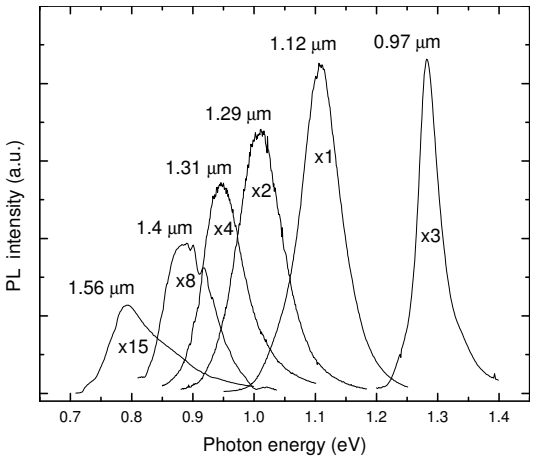

Figure 5.5. Room temperature photoluminescence of three 6 nm thick $Ga_{0.83}In_{0.17}N_xAs_{1-x}$ quantum wells with 15 nm thick GaAs barrier grown on Ge with 190 nm thick GaAs buffer. The x varies from 0 to about 0.05. Different factors have been used to make figure clearer and are shown within each spectrum.

higher quantum confinement in a GaInNAs QW than in a InGaAs QW [133]. As more nitrogen is introduced, the spectra are redshifted and due to the increased density of crystal defects the PL intensity is decreased [134].

In Fig. 5.6 the nitrogen content vs. PL photon energy is showed for the $Ga_{0.83}In_{0.17}N_xAs_{1-x}$ samples. The nitrogen content was estimated from the BAC model. Also the samples discussed in publication VII with the indium content of 20 % are shown in the figure. The sample with photon energy of about 0.79 eV, (i.e. 1.56 µm) shows nitrogen incorporation of about 5 %. The nitrogen content is considered fairly high because in the MOVPE technique the incorporation of nitrogen into InGaAs layers is even more difficult than into the GaAs layers. The overall reason for the low incorporation efficiency of nitrogen into InGaAs is suspected to be the surface segregation of indium that creates surface layer with excess indium enhancing desorption of nitrogen adatoms [126, 135]. Fig. 5.7 shows the effect of the DMHz/TBAs molar flow ratio on the nitrogen incorporation. The relative TBAs/III molar flow ratio is also shown in the parentheses next to each data point in the figure. With higher DMHz flows a smaller TBAs/III molar flow ratio is enough to protect the surface. This enables raising the DMHz/TBAs molar flow ratio by decreasing the TBAs flow. However, GaInNAs layers have a very narrow growth window for V/III in-

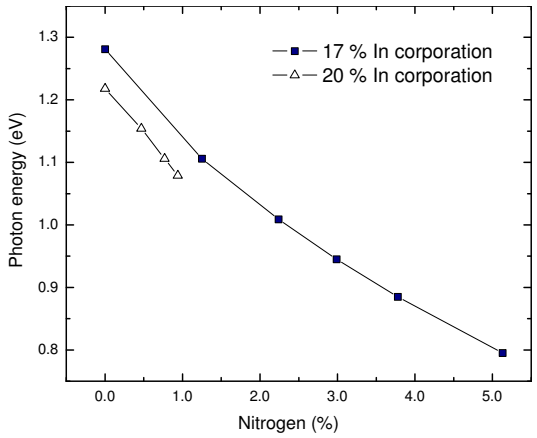

Figure 5.6. Calculated nitrogen contents using BAC model *vs.* photon energy of GaInNAs quantum wells grown on Ge. The strain for the calculations is derived from the HRXRD measurement.

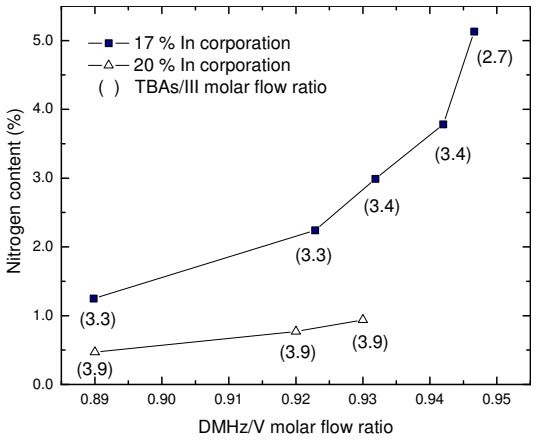

Figure 5.7. Effect of DMHz/V molar flow ratio into nitrogen incorporation in GaInNAs quantum wells grown on Ge. The nitrogen incorporation is derived from the BAC model.

put ratio [134]. In our experiment decreasing the TBAs/III molar flow ratio below 2.5 caused poor crystal quality due to too weak surface protection. It is noteworthy that to introduce few percentages of nitrogen into the layer over 90 % of the total group V gas flow has to be DMHz.

6 Summary

The growth of compound semiconductors on Ge substrates using MOVPE technique was studied. Nucleation and initial growth phases of InAs, InGaAs and GaAs were inspected by AFM. The growth of GaAs on Ge begins by forming three-dimensional islands, which coalesce and form two-dimensional layer if the growth is continued. By adjusting the growth parameters the size, density and uniformity of the coalescence islands can be affected. Significant effort was conducted into optimisations of the growth parameters that favour high areal density and uniformity of the island. The island density has exponential dependency on the growth temperature and is most effectively enhanced by lowering the growth temperature. Using growth temperature below 550°C high island densities over 10^{10} cm^{-3} can be obtained. For the high island density the coalescence of the GaAs islands occurs at small and uniform size and smooth two-dimensional surface is obtained already with small layer thicknesses. To achieve the optimised growth conditions also the input V/III ratio and the growth rate must be carefully chosen. The growth temperature also effects the reconstruction of the germanium surface by controlling the dimerisation. Additive dimerisation is found for the growths initiated above about 600°C and displacive for the growths initiated at lower temperatures. The formation of APDs is prevented if one dimerisation is dominant and the Ge surface has a double step configuration. The double step configuration is obtained using a few degrees misoriented substrate towards ⟨111⟩.

The detailed HRXRD analyses of GaAs/Ge (100) heterostructures are complicated due to the formation of the tilt angle between the (100) lattice planes of Ge and epitaxial GaAs. However, using the parallel setup, presented in this work, scans containing information of the whole structure are successfully obtained. In the parallel setup the X-ray diffraction plane is parallel to the step edges of the Ge substrate and the sample is rotated in the direction of the step edges normal according to the amount of the misorientation. In the HRXRD and in the synchrotron X-ray topography analyses the crystal quality of the grown GaAs/Ge structures was found

nearly perfect and a very low dislocation density of $250 - 500$ cm^{-2} was measured from the topographs of a 650 nm thick GaAs layer. GaAs and Ge have a small lattice constant separation of 0.07 % resulting in strain between Ge and GaAs layer. Small number of misfit dislocations was found in the SXT analyses for the 750 nm thick GaAs layer grown at low growth temperature of 575°C. The critical thickness of about 700 nm is above what is conventionally expected for the GaAs/Ge system. The enhancement in the critical thickness is because of the low growth temperature resulting in smaller thermal stress.

Germanium is an excellent material choice for short wavelength detector applications due to its physical properties and to its availability to fabricate as a very high-purity material. However, conventional manufacturing processes do not alloy finely segmented detector structures on Ge. To gain such novel structures arsenic was appropriately diffused into the Ge wafers in the MOVPE reactor. This enables manufacturing the pixel matrices into germanium. The pixel detector resolution is measured to be as excellent as 220 eV and 400 eV at 5.9 keV and 60 keV, respectively.

The incorporation efficiency of N into GaInAsN quantum well layers is very low. However, in the new approach were Ge substrates are used instead of GaAs substrates the incorporation efficiency of N was found to be more effective. This enhancement results from the small strain compensation introduced by Ge. The low growth temperature of 575°C and the low TBAs/III ratio of 2.7 were used to obtain the long wavelength luminescence maximum 1.56 µm from $Ga_{1-y}In_yN_xAs_{1-x}$ QWs on Ge with a In composition y = 0.17 and a high N composition x = 0.05.

References

[1] S. Strite, M. Ünlü, K. Adomi, G.-B. Gao, A. Agarwal, A. Rockett, H. Morkoç, D. Li, Y. Nakamura and N. Otsuka, *GaAs/Ge/GaAs heterostructure by molecular beam epitaxy*, J. Vac. Sci. Technol. B **8** 1131–1140 (1990).

[2] N. Wu, Q. Zhang, C. Zhu, D. Chan, M. Li, N. Balasubramanian, A. Chin and D.-L. Kwong, *Alternative surface passivation on germanium for metal-oxide-semiconductor applications with high-k gate dielectric*, Appl. Phys. Lett. **85** 4127–4129 (2004).

[3] H. Shang, H. Okorn-Schimdt, J. Ott, P. Kozlowski, S. Steen, E. Jones, H. Wong and W. Hanesch, *Electrical Characterization of Germanium p-Channel MOSFETs*, IEEE Electron Device Lett. **24** 242–244 (2003).

[4] C. Chui, S. Ramanathan, B. Triplett, P. McIntyre and K. Saraswat, *Germanium MOS Capacitors Incorporating Ultrathin High-k Gate Dielectric*, IEEE Electron Device Lett. **23** 473–475 (2002).

[5] D. Schreurs, C. van Niekerk, R. Vandersmissen and G. Borghs, *Development of Extraction and Optimization Based Large-Signal Models for Thinned Metamorphic High- Electron Mobility Transistors on Germanium*, Int. J. RF and Microwave CAE **12** 439–447 (2002).

[6] R. Fischer, H. Morkoç, D. A. Neumann, H. Zabel, C. Choi, N. Otsuka, M. Longerbone and L. Erickson, *Material properties of high-quality GaAs epitaxial layers grown on Si substrates*, J. Appl. Phys. **60** 1640–1647 (1986).

[7] T. Ueda, S. Nishi, Y. Kawarada, M. Akiyama and K. Kaminishi, *Effects of the Substrate Offset Angle on the Growth of GaAs on Si Substrate*, Jpn. J. Appl. Phys. **25** L789–L791 (1986).

[8] D. Biegelsen, F. Ponce, A. Smith and J. Tramontana, *Initial stages of epitaxial growth of GaAs on (100) silicon*, J. Appl. Phys. **61** 1856–1859 (1987).

[9] H. Noge, H. Kano, M. Hashimoto and I. Igarashi, *Antiphase domains in GaAs grown on a (001)-oriented Si substrate by molecular-beam epitaxy*, J. Appl. Phys. **64** 2246–2248 (1988).

[10] S. Onozawa, T. Uedo and masahiro Akiyama, *Initial Stage of MOCVD Growth of GaAs on Si*, J. Cryst. Growth **93** 443–448 (1988).

[11] T. Soga, T. George, T. Jimbo and M. Umeno, *Initial Growth Mechanism for GaAs and GaP on Si Substrate by Metalorganic Chemical Vapor Deposition*, Jpn. J. Appl. Phys. **30** 3471–3474 (1991).

[12] M. Currie, S. Samavedam, T. Langdo, C. Leitz and E. Fitzgerald, *Controlling threading dislocation densities in Ge on Si using graded SiGe layers and chemical-mechanical polishing*, Appl. Phys. Lett. **72** 1718–1720 (1998).

[13] C. Andre, J. Boeckl, C. Leitz, M. Currie, T. Langdo, E. Fitzgerald and S. Ringel, *Low-temperature GaAs films grown on Ge and Ge/SiGe/Si substrates*, J. Appl. Phys. **94** 4980–4985 (2003).

[14] J. Carlin, S. Ringel, E. Fitzgerald, M. Bulsara and B. Keyes, *Impact of GaAs buffer thickness on electronic quality of GaAs grown on graded Ge/GeSi/Si substrates*, Appl. Phys. Lett. **76** 1884–1886 (2000).

[15] N. Chand, J. Klem, T. Henderson and H. Morkoç, *Diffusion of As and Ge during growth of GaAs on Ge substrate by molecular beam epitaxy: Its effect on the device electrical characterics*, J. Appl. Phys **59** 3601–3604 (1986).

[16] P. Modak, M. Hudait, S. Hardikar and S. Krupanidhi, *OMVPE growth of undoped and Si-doped GaAs epitaxial layers on Ge*, J. Cryst. Growth **193** 501–509 (1998).

[17] G. Timo, C. Flores, B. Bollani, D. Passoni, C. Bocchi, P. Franzosi, L. Lazzarini and G. Salviati, *The effect of the growth rate on the low pressure metalorganic vapour phase epitaxy of GaAs/Ge heterostructures*, J. Cryst. Growth **125** 440–448 (1992).

[18] R. Fischer, W. Masselink, J. Klem, T. Henderson, T. McGlinn, H. Morkoç, J. Mazur and J. Washburn, *Growth and properties of GaAs/AlGaAs on nonpolar substrates using molecular beam epitaxy*, J. Appl. Phys. **58** 374–381 (1985).

[19] P. Iles, Y.-C. M. Yeh, F. Ho, C.-L. Chu and C. Cheng, *High-Efficiency (>20% AMO) GaAs Solar Cells Grown on Inactive-Ge substrates*, IEEE Electron Device Lett. **11** 140–142 (1990).

[20] J. Chen, M. L. Ristow, J. Cubbage and J. Werthen, *Effects of metalorganic chemical vapor deposition growth conditions on the GaAs/Ge solar cell properties*, Appl. Phys. Lett. **58** 2282–2284 (1991).

[21] Y. Li, L. Lazzarini, L. Giling and G. Salviati, *On the sublattice location of GaAs grown on Ge*, J. Appl. Phys. **76** 5748–5753 (1994).

[22] Y. Li, G. Salviati, M. Bongers, L. Lazzarini, L. Nasi and L. Giling, *On the formation of antiphase domains in the system of GaAs on Ge*, J. Cryst. Growth **163** 195–202 (1996).

[23] Y. Li and L. Giling, *A closer study on the self-annihilation of antiphase boundaries in GaAs epilayers*, J. Cryst. Growth **163** 203–211 (1996).

[24] L. Lazzarini, L. Nasi, G. Salviati, C. Fregonara, Y. Li, L. Giling, C. Hardingham and D. Holt, *Antiphase disorder in GaAs/Ge heterostructure for solar cells*, Micron **31** 217–222 (2000).

[25] M. Hudait and S. Krupanidhi, *Atomic force microscopy study of surface morphology in Si-doped epi-GaaAs on Ge substrates: effect of off orientation*, Materials Research Bulletin **35** 909–919 (2000).

[26] N. Cho and C. Carter, *Formation faceting and interaction behaviors of antiphase boundaries in GaAs thin films*, J. Materials Science **36** 4209–4222 (2001).

[27] R. Tyagi, M. Singh, M. Thirumavalavan, T. Srinivasan and S. Agarwal, *The Influence of As and Ga Prelayers on the Metal-Organic Chemical Vapor Deposition of GaAs/Ge*, J. Elect. Mat. **31** 234–237 (2002).

[28] M. Hudait and S. Krupanidhi, *Self-annihilation of antiphase boundaries in GaAs epilayers on Ge substrates grown by metal-organic vapor-phase epitaxy*, J. Appl. Phys. **89** 5972–5979 (2001).

[29] J. Derluyn, K. Dessein, G. Flamand, Y. Mols, J. Poortmans, G. Borghs and I. Moerman, *Comparison of MOVPE grown GaAs solar cells using different substrates and group-V precursors*, J. Cryst. Growth **247** 237–244 (2003).

[30] C.-A. Chang, *Interface morphology of epitaxial growth of Ge on GaAs and GaAs on Ge by molecular beam epitaxy*, J. Appl. Phys. **53** 1253–1255 (1982).

[31] J. Neave, P. Larsen, B. Joyce, J. Gowers and J. van der Veen, *Some observations on Ge:GaAs(001) and GaAs:Ge(001) interfaces and films*, J. Vac. Sci. Technol. B **1** 668–674 (1983).

[32] P. Petroff, *Nucleation and growth of GaAs on Ge and the structure of antiphase boundaries*, J. Vac. Sci. Technol. B **4** 874–877 (1986).

[33] S. Strite, D. Biswas, K. Adomi and H. Morkoç, *Study of sublattice orientation of GaAs on Ge*, J. Appl. Phys. **67** 1609–1612 (1990).

[34] E. Fitzgerald, J. Kuo, Y. Xie and P. Silverman, *Necessity of Ga prelayers in GaAs/Ge growth using gas-source molecular beam epitaxy*, Appl. Phys. Lett. **64** 733–735 (1994).

[35] S. Ting, E. Fitzgerald, R. Sieg and S. Ringel, *Range of Defect Morphologies on GaAs Grown on Offcut (001) Ge Substrates*, J. Elect. Mat. **27** 451–461 (1998).

[36] A. Gutakovsky, A. Katkov, M. Kotkov, O. Pcheluakov and M. Revenko, *Effect of Ga predeposition layer on the growth of GaAs vicinal Ge(001)*, J. Cryst. Growth **201/202** 232–235 (1999).

[37] W. Li, S. Laaksonen, J. Haapamaa and M. Pessa, *Growth of device-quality GaAs layer directly on (001) Ge substrates by both solid-source and gas-source MBE*, J. Cryst Growth **227-228** 104–107 (2001).

[38] A. Wan, V. Menon, S. Forrest, D. Wasserman, S. Lyon and A. Kahn, *Characterization of GaAs grown by molecular beam epitaxy on vicinal Ge(100) substrates*, J. Vac. Sci. Technol. B **22** 1893–1898 (2004).

[39] H. Manasevit, *Single-crystal gallium arsenide on insulating substrates*, Appl. Phys. Lett. **12** 156–159 (1968).

[40] C. Larsen, N. Buchan, S. Li and G. Stringfellow, *Decomposition mechanism of tertiarybutylarsine*, J. Cryst. Growth **94** 663–672 (1989).

[41] A. Jones, *Metalorganic precursors for vapour phase epitaxy*, J. Cryst. Growth **129** 728–773 (1993).

[42] F. Salomonsson, C. Asplund, S. Mogg, G. Plaine, P. Sundgren and M. Hammar, *Low-treshold high-temperature operation of 1.2 μm InGaAs vertical cavity lasers*, Electron. Lett. **37** 957–958 (2001).

[43] A. Moto, S. Tanaka, N. Ikoma, T. Tanabe, S. Takagishi, M. Takagishi and T. Katsuyama, *Metalorganic Vapor Phase Epitaxial Growth of GaNAs Using Tertiarybutylarsine (TBA) and Dimethylhydrazine (DMHy)*, Jpn. J. Appl. Phys. **38** 1015–1018 (1999).

[44] G. Solomon, J. Trezza and J. Harris, *Substrate temperature and monolayer coverage effects on epitaxial ordering of InAs and InGaAs islands on GaAs*, Appl. Phys. Lett. **66** 991–993 (1995).

[45] J. Oshinowo, M. Nishioka, S. Ishida and Y. Arakawa, *Highly uniform InGaAs/GaAs quantum dots (∼15 nm) by metalorganic chemical vapor deposition*, Appl. Phys. Lett. **65** 1421–1423 (1994).

[46] N. Ledentsov, J. Böhrer, D. Bimberg, I. Kochnev, M. V. Maximov, P. Kop'ev, Z. Alferov, A. Kosogov, S. Ruvimov, P. Werner and U. Gösele, *Formation of coherent superdots using metal-organic chemical vapor deposition*, Appl. Phys. Lett. **69** 1095–1097 (1996).

[47] F. Heinrichsdorff, A. Krost, N. K. abd Ming-Hua Mao, M. Grundmann, D. Bimberg, A. Olegovich and P. Werner, *InAs/GaAs Quantum Dots Grown by Metalorganic Chemical Vapor Deposition*, Jpn. J. Appl. Phys. **36** 4129–4133 (1997).

[48] R. Leon, C. Lobo, J. Zou, T. Romeo and D. Cockayne, *Stable and metastable InGaAs/GaAs Island Shapes and Surfactantlike Suppression of the Wetting Transformation*, Phys. Rev. Lett. **81** 2486–2489 (1998).

[49] A. Passaseo, R. Rinaldi, M. Longo, S. Antonaci, A. Convertino, R. Cingolani, A. Taurino and M. Catalano, *Structural study of InGaAs/GaAs quantum dots grown by metalorganic chemical vapor deposition for optoelectronic applications at 1.3 μm*, J. Appl. Phys. **89** 4341–4348 (2001).

[50] J. Moison, F. Houzay, F. Barthe, L. Leprince, E. Andre and O. Vatel, *Self-organized growth of regular nanometer-scale InAs dots on GaAs*, Appl. Phys. Lett. **64** 196–198 (1994).

[51] O. Brandt, L. Tapfer, K. Ploog, R. Bierwolf, M. Hohenstein, F. Philipp, H. Lage and A. Heberle, *InA quantum dots in a single-crystal GaAs matrix*, Phys. Rev. B **44** 8044–8053 (1991).

[52] D. Leonard, M. Krishnamurthy, C. Reaves, S. Denbaars and P. Petroff, *Direct formation of quantum-sized dots from uniform coherent islands of InGaAs on GaAs surfaces*, Appl. Phys. Lett. **63** 3203–3205 (1993).

[53] N. Ledentsov, V. Shchukin, M. Grundmann, N. Kirstaedter, J. Böhrer, O. Schmidt, D. Bimberg, V. Ustinov, A. Egorov, A. Zhukov, P. Kop'ev, S. Zaitsev, N. Gordeev, Z. Alferov, A. Borovkov, A. Kosogov, S. Ruvimov, P. Werner, U. Güsele and J. Heydenreich, *Direct formation of vertically coupled quantum dots in Stranski-Krastanow growth*, Phys. Rev. B **54** 8743–8750 (1996).

[54] Y. Sugiyama, Y. Nakata, K. Imamura, S. Muto and N. Yokoyama, *Stacked InAs Self-Assembled Quantum Dots on (001) GaAs grown by molecular beam epitaxy*, Jpn. J. Appl. Phys. **35** 1320–1324 (1996).

[55] M. Colocci, F. Bogani, L. Carraresi, R. Mattolini, A. Bosacchi, S. Franchi, P. Frigeri, M. Rosa-Clot and S. Taddei, *Growth patterns of self-assembled InAs quantum dots near the two-dimensional to three-dimensional transition*, Appl. Phys. Lett. **70** 3140–3142 (1997).

[56] J. Marquez, L. Geelhaar and K. Jacobi, *Atomically resolved structure of InAs quantum dots*, Appl. Phys. Lett. **78** 2309–2311 (2001).

[57] K. Jacobi, *Atomic structure of InAs quantum dots on GaAs*, Progress in Surface Science **71** 185–215 (2003).

[58] D. Leonard, K. Pond and P. Petroff, *Critical layer thickness for self-assembled InAs islands on GaAs*, Phys. Rev. B **50** 11687 (1994).

[59] T. Soga, T. Suzuki, M. Mori, T. Jimbo and M. Umeno, *The effects of the growth parameters on the initial stage of epitaxial growth of GaP on Si by metalorganic chemical vapor depositon*, J. Cryst. Growth **132** 134–140 (1993).

[60] T. Suzuki, T. Soga, T. Jimbo and M. Umeno, *Growth mechanism of GaP on Si by MOVPE*, J. Cryst. Growth **115** 158–163 (1991).

[61] Y.-W. Mo, D. Savage, B. Swartzentruber and M. Lagally, *Kinetic Pathway in Stranski-Krastanov Growth of Ge on Si(001)*, Phys. Rev. Lett. **65** 1020–1023 (1990).

[62] Z. Gai, W. Yang, T. Sakurai and R. Zhao, *Heteroepitaxy of germanium on Si(103) and stable surfaces of germanium*, Phys. Rev. B **59** 13009–13013 (1999).

[63] L. Bobb, H. Holloway, K. Maxwell and E. Zimmerman, *Oriented growth of Semiconductors. III. Growth of Gallium Arsenide on Germanium*, J. Appl. Phys. **37** 4687–4693 (1966).

[64] K. Mizuguchi, N. Hayafuji, S. Ochi, T. Murotani and K. Fujikawa, *MOCVD GaAs growth on Ge (100) and Si (100) substrates*, J. Cryst. Growth **77** 509–514 (1986).

[65] H. Kroemer, *Polar-on-nonpolar epitaxy*, J. Cryst. Growth **81** 193–204 (1987).

[66] M. Kawabe, T. Ueda and H. Takasugi, *Initial Stage and Domain Structure of GaAs Grown on Si(100) by molecular Beam Epitaxy*, Jpn. J. Appl Phys. **26** L114–L116 (1987).

[67] J. Varrio, H. Asonen, J. Lammasniemi, K. Rakennus and M. Pessa, *Model of growth of single-domain GaAs layers on double-domain Si substrates by molecular beam epitaxy*, Appl. Phys. Lett. **55** 1987–1989 (1989).

[68] R. Bringans, D. Biegelsen and L.-E. Swartz, *Atomic-step rearrangement on Si(100) by interaction with arsenic and the implication for GaAs-on-Si epitaxy*, Phys. Rev. B **44** 3054–3063 (1991).

[69] S. Ting and E. Fitzgerald, *Metal-organic chemical vapor deposition of single domain GaAs on Ge/GeSi/Si and Ge substrates*, J. Appl. Phys. **87** 2618–2628 (2000).

[70] P. Pukite and P. Cohen, *Supression of antiphase domains in the growth of GaAs on Ge(100) by molecular beam epitaxy*, J. Cryst. Growth **81** 214–220 (1987).

[71] J. Griffit, J. Kubby, P. Wierenga, R. Becker and J. Vickers, *Tunneling microscopy of steps on vicinal Ge(001) and Si(001) surfaces*, J. Vac. Sci. Technol. A **6** 493–496 (1988).

[72] I. Kamiya, D. Aspnes, H. Tanaka, L. Florez, J. Harbison and R. Bhat, *Surface Science at Atmospheric Pressure: Reconstructions on (001) GaAs in organometallic Chemical Vapor Deposition*, Phys. Rev. Lett. **68** 627–631 (1992).

[73] R. Kaplan, *LEED study of the stepped surface of vicinal Si (100)*, Surface Science **93** 145–158 (1980).

[74] M. Bongers, Y. Li, J. te Nijenhuis and L. Giling, *Structural analysis of $In_xGa_{1-x}As$ grown on Ge by low pressure metalorganic chemical vapour deposition*, J. Cryst. Growth **162** 7–14 (1996).

[75] H. Nagai, *Structure of vapor-deposited GaInAs crystals*, J. Appl. Phys. **45** 3789–3794 (1974).

[76] P. Auvray, M. Baudet and A. Regreny, *X-ray diffraction effects in Ga and Al arsenide structures MBE-grown on slightly misoriented GaAs (001) substrates*, J. Cryst. Growth **95** 288–291 (1989).

[77] W. Bartels, *Characterization of thin layers on perfect crystals with a multipurpose high resolution x-ray diffractometer*, J. Vac. Sci. Technol. B **1** 338–345 (1983).

[78] B. Usher, G. Smith, S. Barnett, A. Keir and A. Pitt, *X-ray diffraction determination of a semiconductor epilayer unit cell oriented and distorted arbitrarily*, J. Phys. D: Appl. Phys. **26** A181–A187 (1993).

[79] R. Hess, C. Moore and M. Goorsky, *lattice tilt and relaxation in InGaP/GaAs/Ge solar cells on miscut substrates*, J. Phys. D: Appl. Phys. **32** A16–A20 (1999).

[80] T. Tuomi, K. Naukkarinen and P. Rabe, *Use of Synchrotron Radiation in X-Ray Diffraction Topography*, Phys. stat. sol. (a) **25** 93–106 (1974).

[81] T. Tuomi, *Synchrotron X-ray topography of electronic materials*, J. Synchrotron Rad. **9** 174–178 (2002).

[82] E. Müller, *Structure of Oriented, Vapor-Deposited GaAs Films, Studied by Electron Diffraction*, J. Appl. Phys. **35** 580–585 (1964).

[83] J. Matthews and A. Blakeslee, *Defects in epitaxial multilayers*, J. Cryst Growth **27** 118–125 (1974).

[84] V. Yang, S. Ting, M. Groenert, M. Bulsara, M. Currie, C. Leitz and E. Fitzgerald, *Comparison of luminescent efficiency of InGaAs quantum well structures grown on Si GaAs Ge and SiGe virtual substrates*, J. Appl. Phys. **93** 5095–5102 (2003).

[85] P. Maugne and A. Roth, *X-ray diffraction of relaxed InGaAs heterostructures grown on misoriented (100) GaAs substrates*, Semicond. Sci. Technol. **7** 1–5 (1992).

[86] J. te Nijenhuis, P. van der Wel, E. van Eck and L. Giling, *Misfit dislocation formation in lattice-mismatched III-V heterostructures grown by metal-organic vapour phase epitaxy*, J. Phys. D: Appl. Phys. **29** 2961–2970 (1996).

[87] L. Pavesi and M. Guzzi, *Photoluminescence of AlGaAs alloys*, J. Appl. Phys. **75** 4779–4842 (1994).

[88] M. Nathan and G. Burns, *Recombination Radiation in GaAs*, Phys. Rev. **129** 125–128 (1963).

[89] M. Sturge, *Optical Absorption of Gallium Arsenide between 0.6 and 2.75 eV*, Phys. Rev. **127** 768–773 (1962).

[90] H. Kressel, F. Hawrylo and P. LeFur, *Luminescence due to Ge Acceptors in GaAs*, J. Appl. Phys. **39** 4059–4066 (1968).

[91] E. Williams, *Evidence for Self-Activated Luminescence in GaAs: The Gallium Vacancy-Donor Center*, Phys. Rev. **168** 922–928 (1968).

[92] E. Williams and C. Elliot, *Luminescence studies of a new line associated with germanium in GaAs*, Brit. J. Appl. Phys. (J. Phys. D) **2** 1657–1665 (1969).

[93] H. Kressel, *Radiative Recombination in Melt-Grown n-Type, Ge-doped GaAs*, J. Appl. Phys. **38** 4383–4387 (1967).

[94] M. Bafleur, A. Munoz-Yague, J. Castano and J. Piqueras, *Photoluminescence of molecular beam epitaxially grown Ge-doped GaAs*, J. Appl. Phys. **54** 2630–2634 (1983).

[95] M. Hudait, P. Modak, S. Hardikar and S. Krupanidhi, *Photoluminescence studies on Si-doped GaAs/Ge*, J. Appl. Phys. **83** 4454–4461 (1998).

[96] E. Burstein, *Anomalous optical absorption limit in InSb*, Phys. Rev. **93** 632–633 (1954).

[97] T. Moss, *The Interpretation of the Properties of Indium Antimonide*, Proc. Phys. Soc. B **67** 775–782 (1954).

[98] H. Casey Jr. and F. Stern, *Concentration-dependent absorption and spontaneous emission of heavily doped GaAs*, Journal of Applied Physics **47** 631–643 (1976).

[99] E. Vainonen-Ahlgren, T. Ahlgren, J. Likonen, S. Lehto, J. Keinonen, W. Li and J. Haapamaa, *Identification of vacancy charge states in diffusion of arsenic in germanium*, Appl. Phys. Lett. **77** 690–692 (2000).

[100] D. Friedman and J. Olson, *Analysis of Ge Junctions for GaInP/GaAs/Ge Three-junction Solar Cells*, Prog. Photovolt: Res. Appl. **9** 179–189 (2001).

[101] M. Yamaguchi, T. Takamoto, K. Araki and N. Ekins-Daukes, *Multi-junction III-V solar cells: current status and future potential*, Solar Energy **79** 78–85 (2005).

[102] N. Karam, R. King, T.Cavicchi, D. krut, J. Ermer, M.Haddad, L. Cai, D. Joslin, M. Takahashi, J. Eldredge, W. Nishikawa, D. Lillington, B. Keyes and R. Ahrenkiel, *Development and Characterization of High-Efficiency $Ga_{0.5}In_{0.5}P/GaAs/Ge$ Dual- and Triple-Junction Solar Cells*, IEEE Transactions on Electron Devices **46** 2116–2125 (1999).

[103] J. Chen, M. Ristow, J. Cubbage and J. Werthen, *High-efficiency GaAs solar cells grown on passive-Ge substrates by atmospheric pressure OMVPE*, Photovoltaic Specialists Conference, Conference Record of the Twenty Second IEEE 133–136 (1991).

[104] S. Wojtczuk, S. Tobin, M. Sanfacon, V. Haven, L. Geoffroy and S. Vernon, *Monolithic two-terminal GaAs/Ge tandem space concentrator cells*, Photovoltaic Specialists Conference, Conference Record of the Twenty Second IEEE 73–79 (1991).

[105] M. Weyers, M. Sato and H. Ando, *Red Shift of Photoluminescence and Absorption in Dilute GaAsN Alloy Layers*, Jpn. J. Appl. Phys. **31** L853–L855 (1992).

[106] M. Kondow, K. Uomi, A. Niwa, T. Kitatani, S. Watahiki and Y. Yazawa, *GaInNAs: A Novel Material for Long-Wavelength-Range Laser Diodes with Excellent High-Temperature Performance*, Jpn. J. Appl. Phys. **35** 1273–1275 (1996).

[107] D. Friedman, J. Geisz, S. Kurtz and J. Olson, *1-eV solar cells with GaInNAs active layer*, J. Cryst. Growth **195** 409–415 (1998).

[108] S. Kurtz, A. Allerman, E. Jones, J. Gee, J. Banas and B. Hammons, *InGaAsN solar cells with 1.0 eV band gap, lattice matched to GaAs*, Appl. Phys. Lett. **74** 729–731 (1999).

[109] R. King, P. Colter, D. Joslin, K. Edmondson, D. Krut, N. Karam and S. Kurtz, *High-Voltage, Low-Current GaInP/GaInP/GaAs/GaInNAs/Ge Solar Cells*, Photovoltaic Specialists Conference, Conference Record of the Twenty-Ninth IEEE 852–855 (2002).

[110] F. Dimroth, C. Baur, A. Bett, K. Volz and W. Stolz, *Comparison of dilute nitride growth on a single- and 8×4-inch multiwafer MOVPE*

system for solar cell applications, J. Cryst. Growth **272** 726–731 (2004).

[111] J. Geisz, D. Friedman, J. Olson, S. Kurtz and B. Keyes, *Photocurrent of 1 eV GaInNAs lattice-matched to GaAs*, J. Cryst Growth **195** 401–408 (1998).

[112] M. D'Hondt, Z.-Q. Yu, B. Depreter, C. Sys, I. Moerman, P. Demeester and P. Mijlemans, *High quality InGaAs/AlGaAs lasers grown on Ge substrates*, J. Cryst. Growth **195** 655–659 (1998).

[113] M. D'Hondt, P. Modak, D. Delbeke, I. Moerman, P. V. Daele, R. Baets, P. Demeester and P. Mijlemans, *4mW micro cavity LED at 650nm on germanium substrates*, Light-Emitting Diodes: Research, Manufacturing and Applications IV **3938** 196–204 (2000).

[114] P. Altieri, A. Jaeger, P. Stauss, T. Pietzonka and K. Streubel, *Efficiency and reliability of AlInGaP LEDs grown on germanium substrates*, Light-Emitting Diodes: Research, Manufacturing and Applications IX **5739** 93–101 (2005).

[115] P. Navaretti, H. Hopkinson, M. Gutierrez, J. Davis, G. Hill, M. Herrera, D. Gonzalez and R. Garcia, *Improvement in the optical quality of GaInNAs/GaInAs quantum well structures by interfacial strain reduction*, IEE Proc.-Optoelectron, **151** 301–304 (2004).

[116] M. Behet, J. D. Boeck, G. Borghs and P. Mijlemans, *High-performance InAs quantum well Hall sensors on germanium substrates*, Electronics Lett. **34** 2273–2274 (1998).

[117] L. Darken and C. Cox, *Semiconductors and Semimetals*, Academic Press, vol. 43, pages 23–83 (1995).

[118] R. Anderson, *Experiments on Ge-GaAs heterojunctions*, Solid-State Electronics **5** 341–351 (1962).

[119] M. Hudait and S. Krupanidhi, *Growth, optical, and electron transport studies across isotype n-GaAs/n-Ge heterojunctions*, J. Vac. Sci. Technol. B **17** 1003–1010 (1999).

[120] W. Bi and C. Tu, *Bowing parameter of the band-gap energy of* GaN_xAs_{1-x}, Appl. Phys. Lett. **70** 1608–1610 (1997).

[121] S. Francoeur, G. Sivaraman, Y. Qiu, S. Nikishin and H. Temkin, *Luminescence of as-grown and thermally annealed GaAsN/GaAs*, Appl. Phys. Lett. **72** 1857–1859 (1998).

[122] M. Kondow, K. Uomi, K. Hosomi and T. Mozume, *Gas-Source Molecular Beam Epitaxy of GaN_xAs_{1-x} Using a N Radical as the N Source*, Jpn. J. Appl. Phys. **33** L1056–L1058 (1994).

[123] C. Skierbiszewski, P. Perlin, P. Wisniewski, W. Knap, T. Suski, W. Walukiewicz, W. Shan, K. Yu, J. Ager, E. Haller, J. Geisz and J. Olson, *Large, nitrogen-induced increase of the electron effective mass in $In_yGa_{1-y}N_xAs_{1-x}$*, Appl. Phys. Lett. **76** 2409–2411 (2000).

[124] P. Hai, W. Chen, I. Buyanova, H. Xin and C. Tu, *Direct determination of electron effective mass in GaNAs/GaAs quantum wells*, Appl. Phys. Lett. **77** 1843–1845 (2000).

[125] D. Friedman, A. Norman, J. Geisz and S. R. Kurtz, *Comparison of hydrazine, dimethylhydrazine, and t-butylamine nitrogen sources for MOVPE growth of GaInNAs for solar cells*, J. Cryst. Growth **208** 11–17 (2000).

[126] D. Friedman, J. Geisz, S. Kurtz, J. Olson and R. Reedy, *Nonlinear dependence of N incorporation on In content in GaInNAs*, J. Cryst. Growth **195** 438–443 (1998).

[127] K. Nakahara, M. Kondow, T. Kitatani, M. Larson and K. Uomi, *1.3-μm Continuous-Wave Lasing Operation in GaInNAs Quantum-Well Lasers*, IEEE Photonics Technology Lett. **10** 487–488 (1998).

[128] S. Sato, Y. Osawa, T. Saitoh and I. Fujimura, *Room-temperature pulsed operation of 1.3 μm GaInNAs/GaAs laser diode*, Electronics Lett. **33** 1386–1387 (1997).

[129] T. Kitatani, K. Nakahara, M. Kondow, K. Uomi and T. Tanaka, *A 1.3 μm GaInNAs/GaAs Single-Quantum-Well Laser Diode with a High Characteristic Temperature over 200 K*, Jpn. J. Appl. Phys. **39** L86–L87 (2000).

[130] H. Riechert, A. Y. Egorov, D. Livshits, B. Borchert and S. Illek, *InGaAsN/GaAs heterostructure for long wavelength light-emitting devices*, Nanotechnology **11** 201–205 (2000).

[131] C. Hains, N. Li, K. Yang, X. Huang and J. Cheng, *Room-Temperature Pulsed Operation of Triple-Quantum-Well GaInNAs Lasers Grown on Misoriented GaAs Substrates by MOCVD*, IEEE Photonics Technology Lett. **11** 1208–1210 (1999).

[132] W. Shan, W. Walukiewicz, J. Ager III, E. Haller, J. Geisz, D. Friedman, J. Olson and S. Kurtz, *Band Anticrossing in GaInNAs Alloys*, Phys. Rev. Lett. **82** 1221–1224 (1999).

[133] M. Manasreh, D. Friedman, W. Ma, C. Workman, C. George and G. Salamo, *Photoluminescence of metalorganic-chemical-vapor-deposition-grown GaInNAs/GaAs single quantum wells*, Appl. Phys. Lett. **82** 514–516 (2003).

[134] Z. Pan, T. Miyamoto, D. Schlenker, F. Koyama and K. Iga, *Quality Improvement of GaInNAs/GaAs Quantum Well Growth by Metalorganic Chemical Vapor Deposition Using Tertiarybutylarsine*, Jpn. J. Appl. Phys. **38** 1012–1014 (1999).

[135] I. Suemune, K. Uesugi and T.-Y. Seong, *Growth and structural characterization of III-N-V semiconductor alloys*, Semicond. Sci. Technol. **17** 755–761 (2002).